An integrated remote sensing-GIS approach for the analysis of an open pit in the Carrara marble district, Italy: slope stability assessment through kinematic and numerical methods

Authors: Francioni, M. (a); Salvini, R. (b); Stead, D. (a); Giovannini, R. (b); Riccucci, S. (b); Vanneschi, C. (b); Gullì, D. (c).

(a) Department of Earth Sciences, Simon Fraser University, Burnaby, BC, Canada.
(b) Department of Environment, Earth and Physical Sciences and Centre of Geotechnologies, University of Siena, San Giovanni Valdarno, AR, Italy.
(c) Regione Toscana - Operative Unit of Mining Engineering (U.O.I.M.) AUSL 1 Carrara,Tuscany, Italy

Corresponding author: Francioni, M. Department of Earth Sciences, Simon Fraser University, Burnaby, BC, Canada, 8888 University Drive, Burnaby, B.C., Canada, V5A 1S6. E-mail: mfrancio@sfu.ca. Phone: 778-782-7288

Abstract

Over the last decade, terrestrial laser scanning and digital terrestrial photogrammetry techniques have been increasingly used in the geometrical characterization of rock slopes. These techniques provide innovative remote sensing tools which overcome the frequent problem of rock slope inaccessibility. Comprehensive datasets characterizing the structural geological setting and geometry of the slopes can be obtained. The derived information is very useful in rock slope investigations and finds application in a wide variety of geotechnical and mine operations. In this research an integrated remote sensing – GIS approach is proposed for the deterministic kinematic characterization of the Lorano open pit in the Apuan Alps of Italy. Based on the results of geomatic and engineering geological surveys, additional geomechanical analysis using a 3D finite difference method will be presented in order to provide a better understanding of the role of stress-induced damage on slope performance.

Keywords: Unmanned aerial vehicle; terrestrial laser scanning; GIS, deterministic kinematic analysis, 3D finite difference method; stress-induced damage.

1. Introduction

Surface mining represents a major important economic activity for many countries worldwide. With the high number of people working in the mining industry, safety in the workplace has become an over-riding priority. In this context, the use of new technologies to study and monitor mining and quarrying areas can play a very important role in risk assessment and management.

This paper, developed within the framework of the Italian National Research Project PRIN2009, provides a new approach for the study of open pit quarry slopes based on the integrated use of remote sensing techniques for deterministic stability analyses using combined simple kinematic analysis techniques and three dimensional Finite Difference Method (FDM) stress models. The research describes the case study of the Lorano open pit, characterized by a buttress- shaped remnant from previous excavation activities. The quarry is located in the Carrara district of the Apuan Alps (Italy) which is the most active marble quarrying region in Europe. Here several quarry walls reach hundreds of meters in height and are dominated by natural slopes with very complex morphology. In such an environmental context conventional structural and engineering geological surveys can only be executed at the foot of the slope; therefore, the data obtained from these surveys often provides an incomplete knowledge of the area. An alternative approach would be to have surveys carried out by technicians who are trained in rope access climbing on high rock slopes. There are however limitations and technical difficulties in the implementation of such rope access survey methods, including the close proximity to the quarry wall which compromises visibility and the ability to recognize large-scale geological features, as well as the unavailability of suitable cartographic maps. For these reasons, the use of remote sensing techniques has the potential to significantly increase the information on the geometry and the structural geological setting of quarry slopes.

In this research, two different remote sensing techniques have been used to complement the data obtained from traditional engineering geological surveys. The remote sensing methods used included Terrestrial Laser Scanning (TLS) and Unmanned Aerial Vehicle (UAV) based Digital Terrestrial Photogrammetry (DTP). Several authors have demonstrated the use of TLS and DTP in the study of rock slopes and the advantages that these techniques offer in the structural geological and kinematic analysis of rock slopes [30], [3], [38], [20], [79], [50], [31], [54], [77], [78], [69], [71]. Although UAV technology has been increasingly used in the last few years there remain few published references related to the study of rock slopes [42], [60], [22].

Information gained from these remote sensing techniques was used in this case study for analysing the open pit and overhanging quarry slopes. Two different analyses were carried out; the first, a kinematic analysis to examine the most probable slope failure mechanism and the second a FDM study focused on

understanding the stress distribution within the slope. The kinematic analysis was performed using an integrated remote sensing – Geographic Information System (GIS) approach.
This allowed for a deterministic kinematic analysis based on the geometry of the slope and joint sets. Based on a similar concept, different approaches were used by Brideau et al. [13] and Salvini and Francioni [70]. Brideau et al. [13] compared the wedge intersection vector orientations with the topographic surfaces from a DSM to understand the influence of three-dimensional topography on slope stability analysis. Salvini and Francioni [70] carried out a form of "kinematic back-analysis" using the joint attitudes to identify the areas on the slope that could be affected by future failures.
The FDM analysis was carried out using a simplified 3D model derived from TLS and topographic map at scale of 1:2,000 and focused on characterisation of the rock slope stress distribution. It is known from literature how stress-induced damage due to excavation can be a frequent problem in mining and quarrying and the presence of such stress-induced fractures was observed in the study area in this and previous studies [18], [52] and [17]. These newly generated excavation stress-induced brittle fractures may be an important consideration in the stability of an area and their study could decrease the risk of failure and increase the quality of marble in future extraction works. The principal aim of this study was to understand the stress-induced damage caused by the in-situ stress acting in the area and/or the excavation processes. Several authors have studied the relationship between the acting in-situ stresses, the excavation process and brittle fracturing in excavation areas, particularly in underground mining [14], [15], [28], [29], [16]. In this research the Itasca^{TM} FLAC3D code [49], was used for modelling of excavation induced stress in the quarry slopes.

2. The Lorano open pit case study

The Lorano open pit is located in the Carrara district where marble quarrying is the most important economic activity. Marble extraction in this area has a long history dating back to the Roman Empire (VI – II B.C). Today the Carrara district is the most important marble mining area in Europe with more than 100 active quarries and a production of around 1,000,000 tons/year of blocks and aggregated gravels [18]. Geologically, the Apuan Alps belong to the Northern Apennines and are a compressional fold-thrust belt formed during the Oligocene due to the collision between the Corsica-Sardinia microplate and the Italian peninsula [4], [52], [17].
Evidence for two main tectonic phases can be found in this area. During the first so-called D1 phase (late Oligocene-very early Miocene), there was compression associated with under-thrusting of the Adriatic plate, and deposition following the North-East direction of the Tuscan Nappe and the Ligurids non-metamorphic units. In these conditions, limestone, dated at 180 My, was metamorphosed to marble.

Related to this event, is the formation of the metamorphic foliation (S1) that represents the axial plane of sheath folds (from microscopic to kilometre scale) that characterize the major part of the Apuan Alps. The general S1 direction is relatively constant from N 130^{o} E to N 160^{o} E. This metamorphic foliation represents a direction of weakness in the marble in the Carrara district and, although it is not a true open discontinuity set, it can have an important control on the nucleation and propagation of brittle fracturing [18], [52] and [17]. During the second phase (D2), which started in the early Miocene, compression continued so that all the structures that had developed during D1 were re-folded into complex, antiformal stack geometry with the presence of parasitic folds. Subsequently, compression ended during the last stages of the D2 phase and brittle rather than ductile tectonics occurred. This step was characterised by open and kink folds and normal extension faults with low and high dips. This extensional phase caused stretching, denudation and uplift phenomena, bringing higher and lower structures to the same level. In this context, the Apuan Alps now represent a wide tectonic window within the thickened Apennine Nappe [17].

The Lorano open pit is located in the normal limb of the "Pianza Anticline", between the "Carrara syncline" in the South-West, and the "Vallini syncline" in the North-East. The open pit is characterized by a rock buttress shape, a remnant of previous excavation activities left to ensure the stability of the rock slope to the rear. The marble buttress is accessible from three sides and is approximately 150 m high and between 30 to 50 m wide (Figure 1). In the study area there are two different types of marble outcrops: the "Ordinario marble", that characterizes the buttress, and the "Venato marble" a natural outcrop occurring on the mountain slope above.

Figure 1. Perspective view of the study area: Lorano open pit walls characterized by the rock buttress shape (the scale is indicative only); inset map shows the location of the study area.

3. Geomatic and engineering geological surveys

Most of the open pit walls in the study area are hundreds of meters high and are dominated by natural slopes with very complex morphology which can be a source of danger for workers below. In such an environment, engineering geological surveys are traditionally executed only in accessible areas at the foot of the slope. The data obtained from these surveys fails to provide complete information of the entire slope as required for deterministic slope analysis.

Quarry wall inspections are conducted once a year by rope access climbers but are often constrained by technical difficulties, low visibility compromising the recognition of large-scale geological features, and high cost. Remote sensing techniques can provide an excellent alternative and TLS and DTP in particular are being increasingly used in the study of such areas. Using these techniques it is possible to obtain very detailed information on the structural geological setting and slope geometry, even in the case of inaccessible steep slopes. The integrated use of DTP and TLS for the study of the buttress and the

overhanging slope will be shown in this paper. Special emphasis will be given to the use of UAV for the DTP survey.

3.1 Unmanned Aerial Vehicle for photogrammetric surveys

Digital terrestrial photogrammetry is a remote sensing technique in which the geometric properties of objects are determined by the measurement of photographic images. DTP is used in many different fields, including topographic mapping, architecture, engineering, and, more recently, engineering geology [67], [44], [76], [33], [34]. Slama [73], Linder [56], and Kraus [53] provide further details on the theory of this technique.

Given that pseudo-perpendicular directions of acquisition are necessary owing to the height and steepness of the slopes; traditional remote sensing techniques such as aerial photogrammetry are generally not suitable. The authors have previously discussed the advantages and disadvantages of using different methodologies for photogrammetric data acquisition depending on the slope morphology and the accessibility of rock faces [77], [78], [33], [34]. In this case, considering the elevation and the complex geometry of the buttress (Figure 1), an UAV was used to acquire high spatial resolution images. The survey was carried out by mounting a stabilized digital camera Sony NEX-5N onto a Falcon 8 (Asctec Gmbh) vehicle (Figure 2A and B). The physical CCD frame size of the cameras is 23.5 x 15.6 mm, while the resolution is 16.1 Megapixels.

Based on a flight plan, photographs were automatically taken in order to cover the whole site acquiring vertical strips of images with a minimum 70% overlap and 30% sidelap. Auto-positioning of the UAV was controlled by the integrated inertial measurement unit. Due to the complex morphology of the area and the buttress shape, three different lines-of-sight were used during the photogrammetric survey. Figure 2C shows the orthophoto of the whole open pit and highlights the three different lines-of-sight.

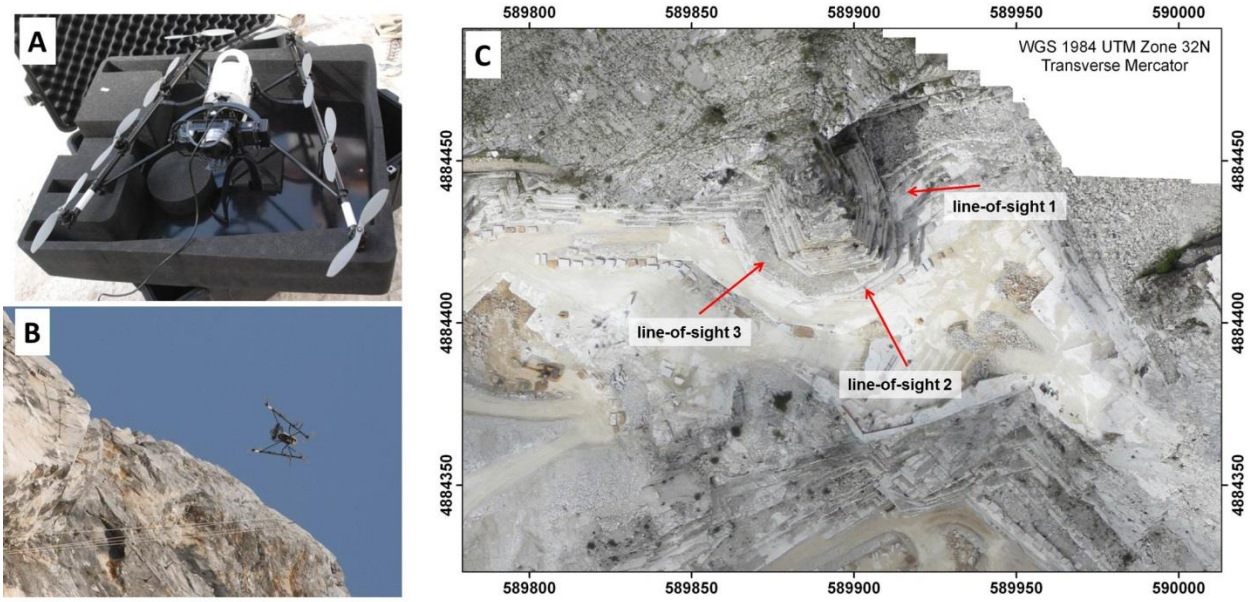

Figure 2. UAV survey: the Falcon 8 with stabilized digital camera Sony NEX-5N (A), vehicle during the flight on the right (B) and orthophoto of the open pit with the three different lines-of-sight used during the photogrammetric survey (C).

Based on the sensor format, horizontal and vertical fields of view varied with the distance from the walls; Table 1 shows the image size of the utilized camera.

	Image size (pixel)	Image size (mm)
Width	3935	333.2
Height	2620	221.8

Table 1. Photogrammetric image size (300 dpi).

With the objective of obtaining very precise output, 91 natural Ground Control Points (GCP) were measured on the buttress walls using a Leica™ TCRP 1203+R1000 reflectorless Total Station. The GCPs are points with known coordinates that must be recognizable on the photographs to facilitate their exterior orientation process (procedure used to define the camera position, rotation and its line-of-sight at the instant of the exposure [73], [56], [53]) that was executed by means of the Leica Photogrammetric Suite (LPS) module of the ERDAS™ IMAGINE software. The Root Mean Square Error (RMSE) in image and ground units (respectively pixel and cm) obtained for each strip during the absolute orientation process is shown in Table 2.

Line-of-sight (degrees to North)	RMSE (image unit, pixel)	RMSE (ground unit, mm)
1 (270)	2.3	33
2 (330)	4.7	48
3 (50)	2.7	35

Table 2. Line-of-sight, image and ground RMSE.

3.2 Terrestrial laser scanning

In addition to DTP, terrestrial laser scanning was used to provide additional geometric information about the buttress and to validate the data obtained from the photogrammetric survey. TLS is a survey technique for rapidly obtaining the geometry of objects with high precision. Several types of laser scanner currently exist with different measurement principles and technical specifications [7], [37]. In this paper, a Riegl™ Z420i laser scanner was used for the survey. This instrument uses time-of-flight technology to determine distances to an object at a maximum distance of about 1 km.

Considering the geometry of the buttress, three point clouds were acquired to limit the occlusions in the output data; the slope scanning resolution was set to 0.07 m at a distance of 300 m. Sturzenegger and Stead [78] and Francioni et al. [34] discussed the complexity of aligning several point clouds in the same reference system through the registration process. The integrated use of Total Station (TS), differential GPS (Global Positioning System) can be adopted to overcome problems related to the registration process. In this case study 15 High-Definition Surveying (HDS) targets were used in the TLS data acquisition whose absolute coordinates were acquired by a TS topographic survey. The targets were automatically recognized by the Leica™ Cyclone software (used also in the TLS data post-processing) so that the registration could be easily computed by assigning them absolute coordinates. The topographic survey played an important role in the registration process and will be described in more detail in the following section.

3.3 Topographic survey

The topographic survey was carried out by means of the Leica™ TCRP 1203+R1000 reflectorless Total Station and two geodetic Leica™ 1200 GPS receivers. They were essential for the acquisition of the HDS targets and GCPs for photogrammetry. During the TS survey, the intersection method was used to relate all the measurements to a unique reference system. Using this technique it was possible to locate the TS in different positions (suitable for the acquisition of HDS targets and GCPs) and to relate all the measurements to the first station (called “Master Station”). The use of the TS and the intersection methods are explained in detail in Francioni et al. [36] and Francioni et al. [34].

The GPS survey was used to determine the absolute coordinates of all the points measured with the TS; to accomplish this, a GPS receiver was set up in the same position as the Master Station and the absolute coordinate of the latter determined. Subsequently, a second GPS receiver was utilized to obtain the zero-Azimuth for the TS and, finally, the absolute coordinates of all the measured points determined. The differential GPS surveys were performed in static modality with an acquisition time of up to 3 hours. The coordinates of the points acquired with this technique were corrected by post-processing procedures using contemporary data recorded by two permanent GPS stations (*Lucca* and *Borgo a Mozzano*). The orthometric heights of the Master and the zero-Azimuth stations were also calculated in collaboration with the Italian Military Geographical Institute.

3.4 Engineering geological survey

In order to provide more information about the structural geological setting of the slope and the characteristics of the rock mass and joint surfaces, an engineering geological survey was carried out. Due to the inaccessibility of the area, it was possible to carry out the scan lines only at the toe of the slope (Figure 3). Seven scan lines were performed and more than 100 surfaces measured. Of these, only 77 were then used for the definition of the main joint sets. The remain surfaces were identified as brittle fractures and, due to their different origin, irregular shape and unreliability in their measurement, they were not considered in the definition of the main joint sets. Data from scan lines was used for the characterization of rock mass according to the Bieniawski Rock Mass Rating (RMR, 1989) method. The RMR system is a rock mass quality classification developed by the South African Council for Scientific and Industrial Research [8] and subsequently updated in 1989 [78]. The Geological Strength Index (GSI) was also estimated based on the rock mass structure and the rock discontinuity surface condition. This method, used widely by the scientific community after its introduction [45], is not intended as a rock mass classification, but rather to reflect the rock mass quality. The GSI value was then applied to estimate the rock mass parameters in the Hoek-Brown strength criterion. The application and limitations of the GSI for underground openings and rock slopes were recently reviewed by Marinos et al. [57] and Hoek and Diederichs [47].

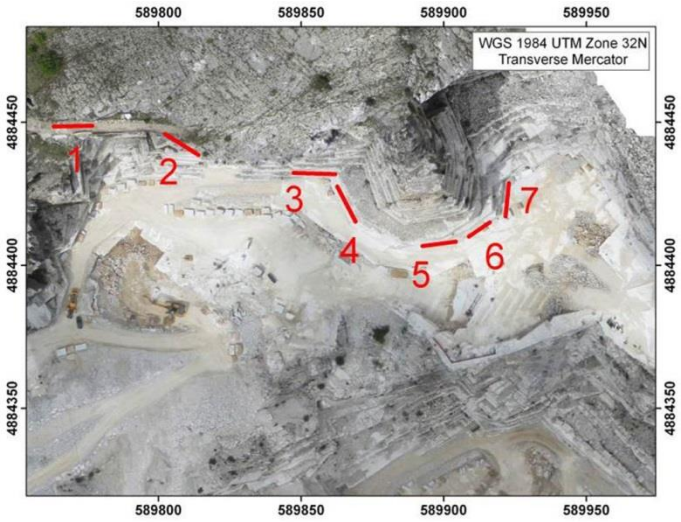

Figure 3. Orthophoto of the open pit with scan lines

4 Data processing and deliverables

In this case study the UAV system, by limiting blind spots, played a very important role in the acquisition of the photographs of the whole study area. The exterior orientation of the photographs was obtained through the use of the 91 GCPs measured by the topographic survey. After the exterior orientation process, a stereographic model of the buttress was built and used for the stereo-interpretation of structural geological features including joint attitude, spacing and trace length. These features were stereo-restituted using the Stereo Analyst module of ERDAS™ IMAGINE; the joint attitude was represented in the stereoscopic model by triangles drawn co-planar with the discontinuities, while the spacing and trace length were shown using 3D lines. Figure 4A shows stereographic representation of the discontinuities measured on the slope using DTP. The three TLS point clouds acquired during the survey were registered using the HDS targets and allowed the construction of a unique 3D model of the buttress. As mentioned above, using the topographic surveys and the intersection method it was possible to align GCPs and HDS targets in the same reference system with an estimated error of approximately 5 mm. In this way, the stereoscopic model from DTP and the TLS 3D model were integrated and used for the construction of a detailed full 3D model with high resolution orthophotos of the buttress (Figure 5).

The DTP approach provides a high level of data interpretability during the stereo-restitution but can be prone to human error. For this reason, the attitude of the discontinuity surfaces and slopes was also extracted from the TLS point clouds using the Leica™ Cyclone software through a semi-automatic procedure. In practice, several points (at least three) representing the surface under investigation must be selected on the point cloud; the software automatically recreates the surface and determines the attitude of

its pole. Figure 4B shows the stereographic representation of the discontinuities measured on the slope using TLS.

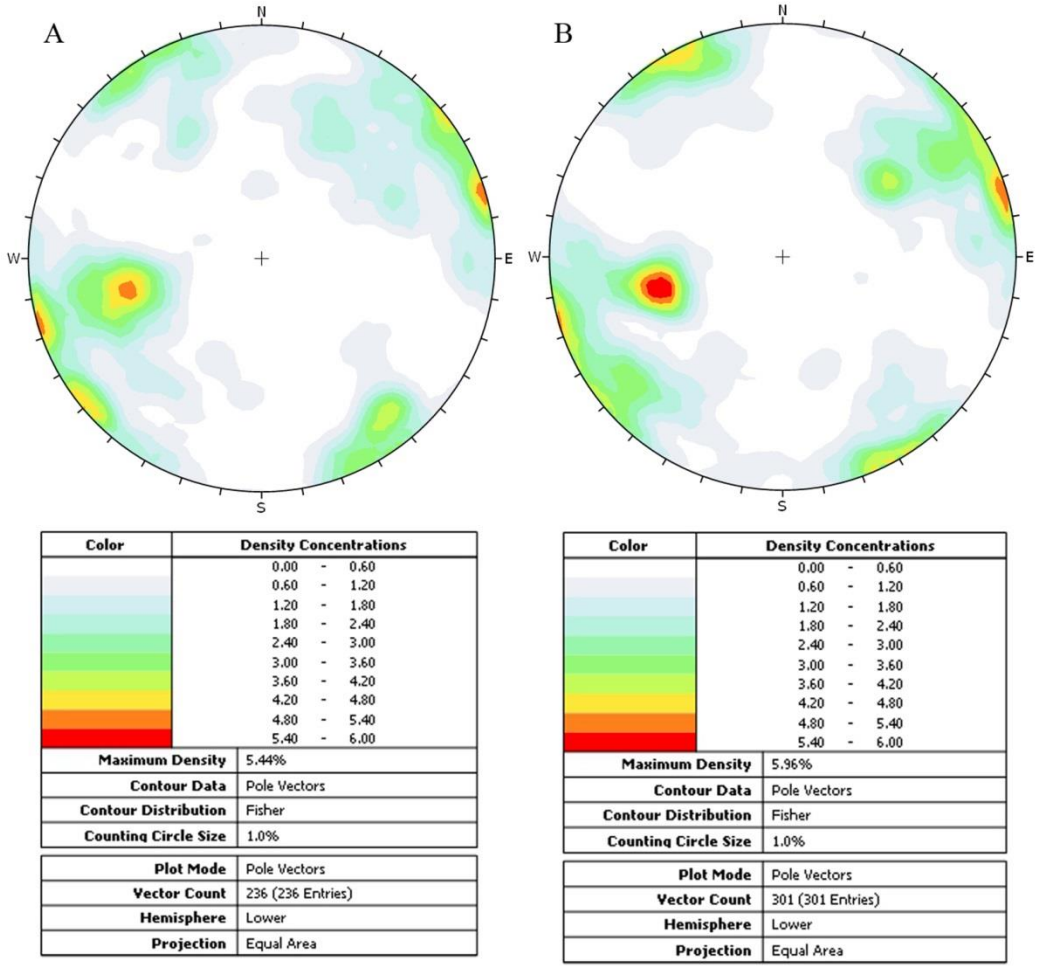

Figure 4. Stereographic representation of measurements obtained from DTP (A) and TLS (B).

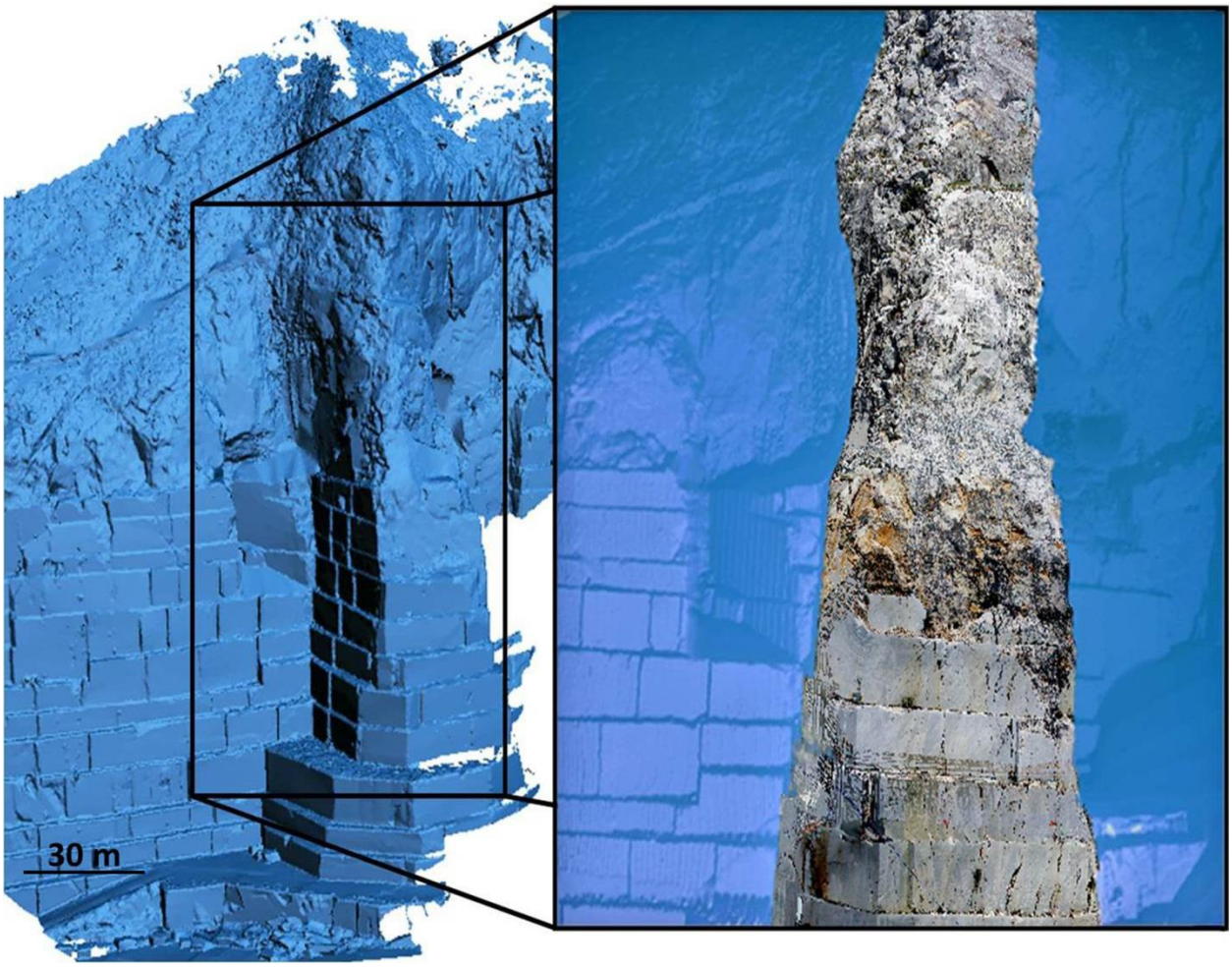

Figure 5. Integration of TLS and UAV photogrammetric data in the construction of the 3D model with aligned orthophotos of the buttress.

All the measurements obtained from TLS and DTP were then integrated in a final stereographic representation and the joint sets determined (Figure 6 and Table 3). K1, K2 and K3 represent the three main joint systems surveyed with these techniques and S1 represent the structures associated with the metamorphic foliation S1 which characterizes the Apuan Alps (see section 2). Table 3 also shows the measurements of spacing and trace length carried out using the remote sensing data. However, due to the difficulty in defining the trace length in the photogrammetric model (especially when the joint spacing is small as often is the case in the Carrara marble district) and to fact that these parameters were required in the following analyses, these measurements should be considered as a preliminary approximate estimation only.

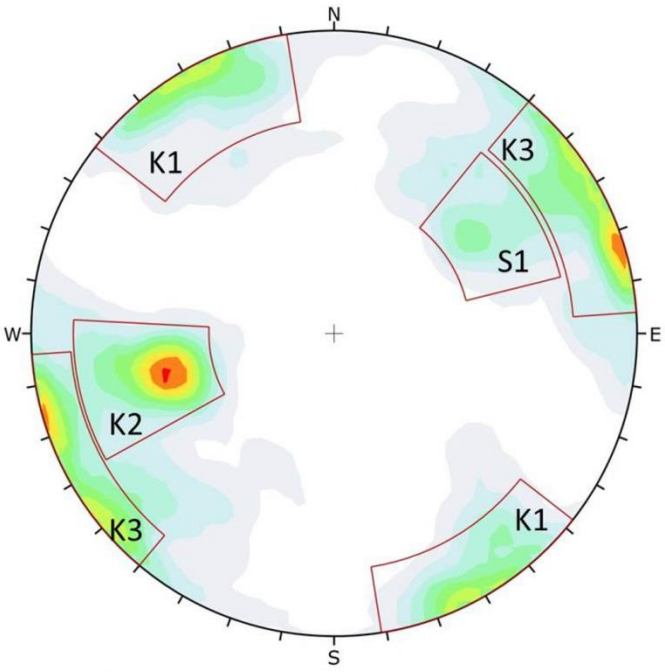

Color	Density Concentrations
	0.00 - 0.60
	0.60 - 1.20
	1.20 - 1.80
	1.80 - 2.40
	2.40 - 3.00
	3.00 - 3.60
	3.60 - 4.20
	4.20 - 4.80
	4.80 - 5.40
	5.40 - 6.00

Maximum Density	5.49%
Contour Data	Pole Vectors
Contour Distribution	Fisher
Counting Circle Size	1.0%

Plot Mode	Pole Vectors
Vector Count	537 (537 Entries)
Hemisphere	Lower
Projection	Equal Area

Figure 6. Integration of measurements obtained from TLS and DTP.

Joint set	Dip (deg)	Dip Direction (deg)	Trace length (m)	Spacing (m)
K1	88	150	10 to 30	1 to 3
K2	54	077	10 to 30	1 to 3
K3	87	243	10 to 30	1 to 3
S1	52	235	2 to 20	1 to 10

Table 3. Data obtained from DTP and TLS.

Conventional engineering geological survey was necessary to assess the accuracy of the joint sets present at the toe of the slope and to physically and mechanically characterise the discontinuities according to the RMR method. Data obtained from this survey is provided in Figure 7 and Table 4; the results gained from

the rock mass rating show a good quality rock mass with an RMR value equal to 76. However, Figure 7 and Table 4 also show that the joint set distribution at the toe of the slope was slightly different to that determined from DTP and TLS. Therefore, data in Table 4 may not be fully representative of all the joint sets illustrated in Table 3 since they refer to different locations within the study area. In fact, GSI values also vary within engineered areas (i.e. open pit) compared to the natural rock outcrops (i.e. the above slope). For this reason and considering in detail the characteristics of the marble the GSI was estimated to vary between 50 and 60 in the natural slope and between 70 and 80 in the open pit face. This is probably due to the degree of weathering of the natural slope surface and to the fact that the joint spacing usually increases with depth.

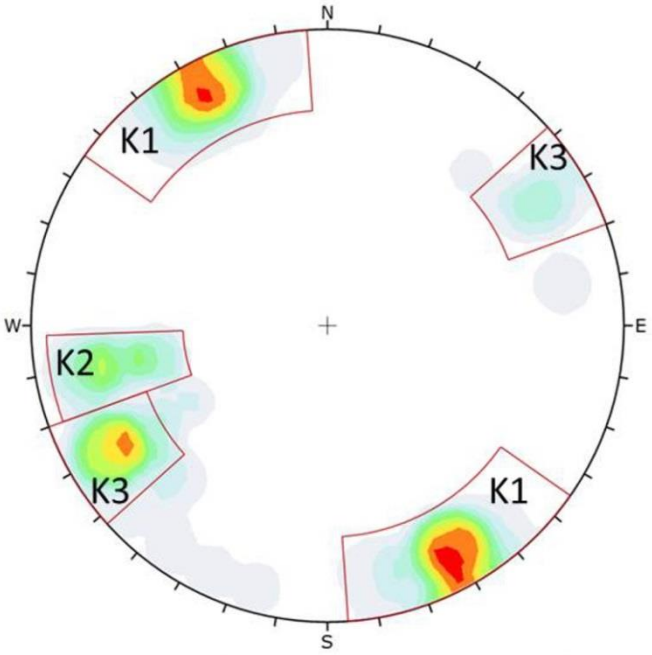

Color	Density Concentrations
	0.00 - 1.50
	1.50 - 3.00
	3.00 - 4.50
	4.50 - 6.00
	6.00 - 7.50
	7.50 - 9.00
	9.00 - 10.50
	10.50 - 12.00
	12.00 - 13.50
	13.50 - 15.00

Maximum Density	14.20%
Contour Data	Pole Vectors
Contour Distribution	Fisher
Counting Circle Size	1.0%

Plot Mode	Pole Vectors
Vector Count	77 (77 Entries)
Hemisphere	Lower
Projection	Equal Angle

Figure 7. Stereographic representation of measurements determined from the conventional engineering geological survey.

Joint set	K1	K2	K3
Dip/Dip Dir	$90^o/332^o$	$71^o/080^o$	$84^o/059^o$
Spacing (m)	1	1	1.5
Trace length (m)	10 to 20	10 to 20	10 to 20
Aperture (mm)	14	9	11
Infill	Absent	Absent	Absent
Weathering	Slight	Slight	Slight
JRC	4	9	5
JCS (MPa)	98	78	83
Water	Medium inflow	Absent	Medium inflow

Table 4. Data obtained from the conventional engineering geological survey (mean values).

During both the remote sensing and engineering geological surveys, brittle (stress-induced) fractures were identified (Figure 8). It is possible to differentiate these structures from pre-existing discontinuities based on their irregular shape and the lower trace length. These characteristics can make their mapping sometimes challenging with a higher degree of uncertainty and, for this reason the measurements related to the stress-induced fractures were kept separate from those associated with joint sets.

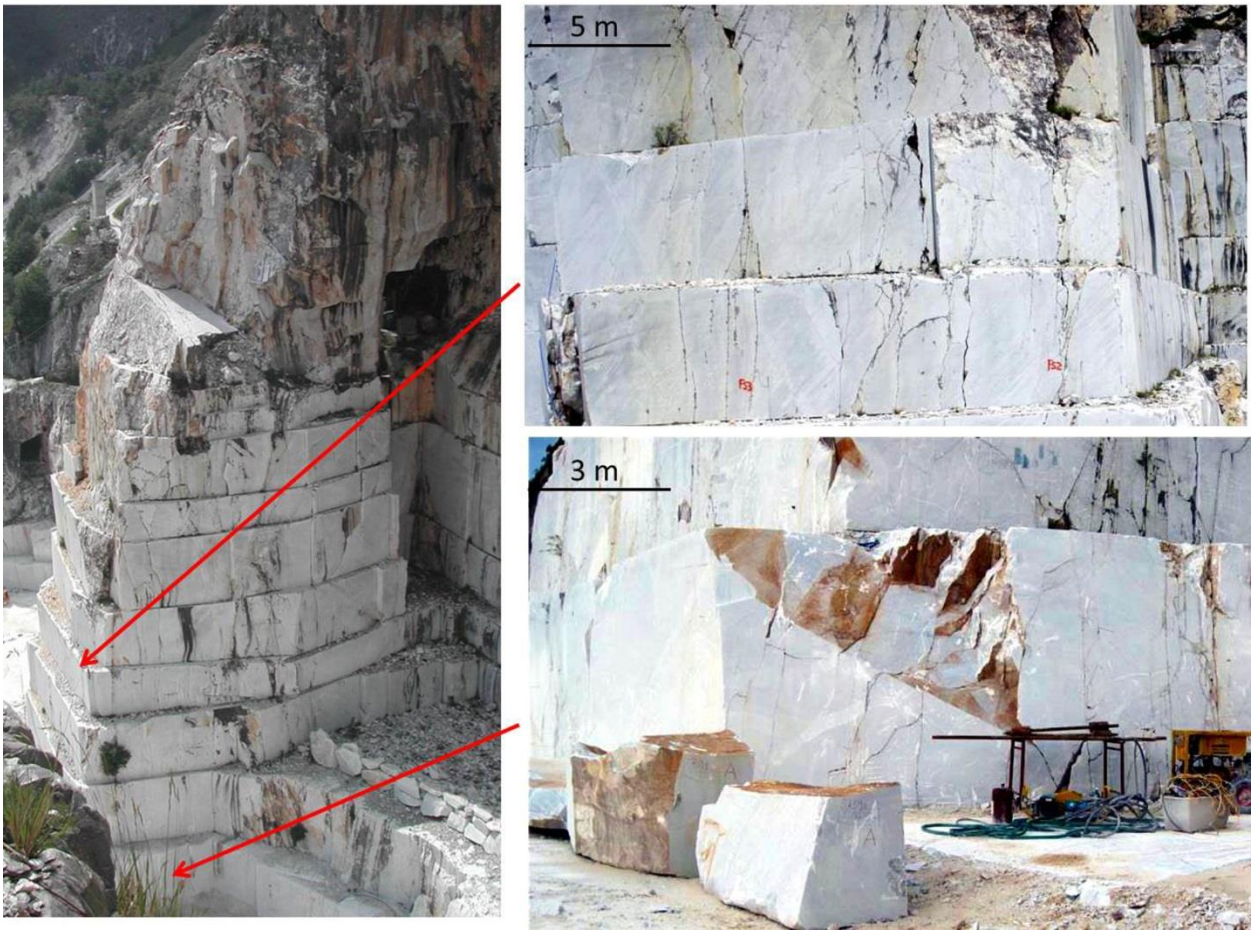

Figure 8. Stress-induced damage noted in the marble buttress during the engineering geological and photogrammetric surveys.

5 GIS and kinematic stability analyses

The kinematic slope stability analysis examines the potential for rock slope failures such as planar, wedge, and toppling due to the presence of unfavourably oriented discontinuities. The analysis considers the relative attitude of the discontinuities and the slope plus the effective friction angle along the joint surfaces. Stereographic projections for the kinematic analysis of these simple failure modes are described in Richards et al. [64] and Hoek and Bray [46]. Various widths of toppling envelope have been proposed by Goodman and Bray [40], Cruden [21], Goodman [39], and Maurenbrecher and Hack [58].

The results of this analysis are strongly influenced by the topography, as already documented by Brideau et al. [13] who proposed the use of software such as Matterocking [50], which compares the wedge intersection vector orientations with the topographic surfaces.

In this research, an integrated remote sensing – GIS analysis approach was proposed to overcome the problem of complex geometry. GIS techniques have been used by several authors for slope stability analysis [82], [81], [84], [85], [23], [6], since they provide various functions for capturing, inputting, manipulating, transferring, visualizing, combining, querying, analysing, modelling, and outputting of the geospatial data. The advent of new survey techniques (such as those used in this research) makes this technique even more attractive because they allow a wider range of data to be analysed. In this research the 3D model and the topographic map at scale of 1:2,000, gained from the TLS, were used in the construction of a simplified Digital Surface Model (DSM) of the pit slope.

Starting from the DSM, a GIS spatial analysis was performed to highlight the dip direction of the slope faces (Figure 9A). Different colours in Figure 10A represent slopes characterized by varying dip direction. Based on the orientation of the slope faces and using the geo-structural data derived from the geomatic and engineering geological surveys, it was possible to perform a kinematic GIS analysis of slope stability. For each slope face, the steepest safe angle was calculated using the stereographic projection of Dips 6.0 software [66]. The knowledge of the steepest safe angle is very useful for understanding the maximum angle that a slope can be quarried at before subject to potential failures due to interaction with discontinuities. This information was integrated with the steepness of the slope in order to ascertain which areas may be affected by failure. Consequently, a further GIS spatial analysis was carried out and the slope steepness calculated (Figure 9B). In this way, all the necessary information was available to understand where failure mechanisms could occur. A supplementary spatial analysis was carried out to combine the steepest safe angle with the slope steepness in order to further refine the results. The friction angle was assumed to be 32^{o} (with 5° of standard deviation) for all the joint systems based on the published literature, [19], [62], [63], [32]. Figure 11 shows the results highlighting the stereographic representation of main joint sets used for the analysis (Figure 10A) and the areas that could be affected by planar (Figure 10B), wedge (Figure 10C), and direct toppling failures (Figure 10D).

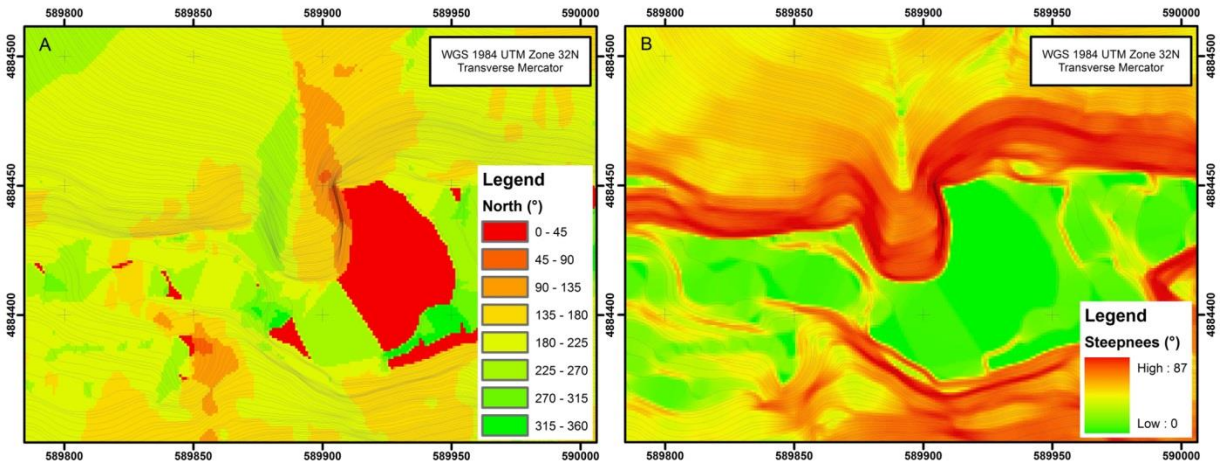

Figure 9. Dip direction of slope faces (A) and slope steepness (B) calculated with GIS spatial analysis.

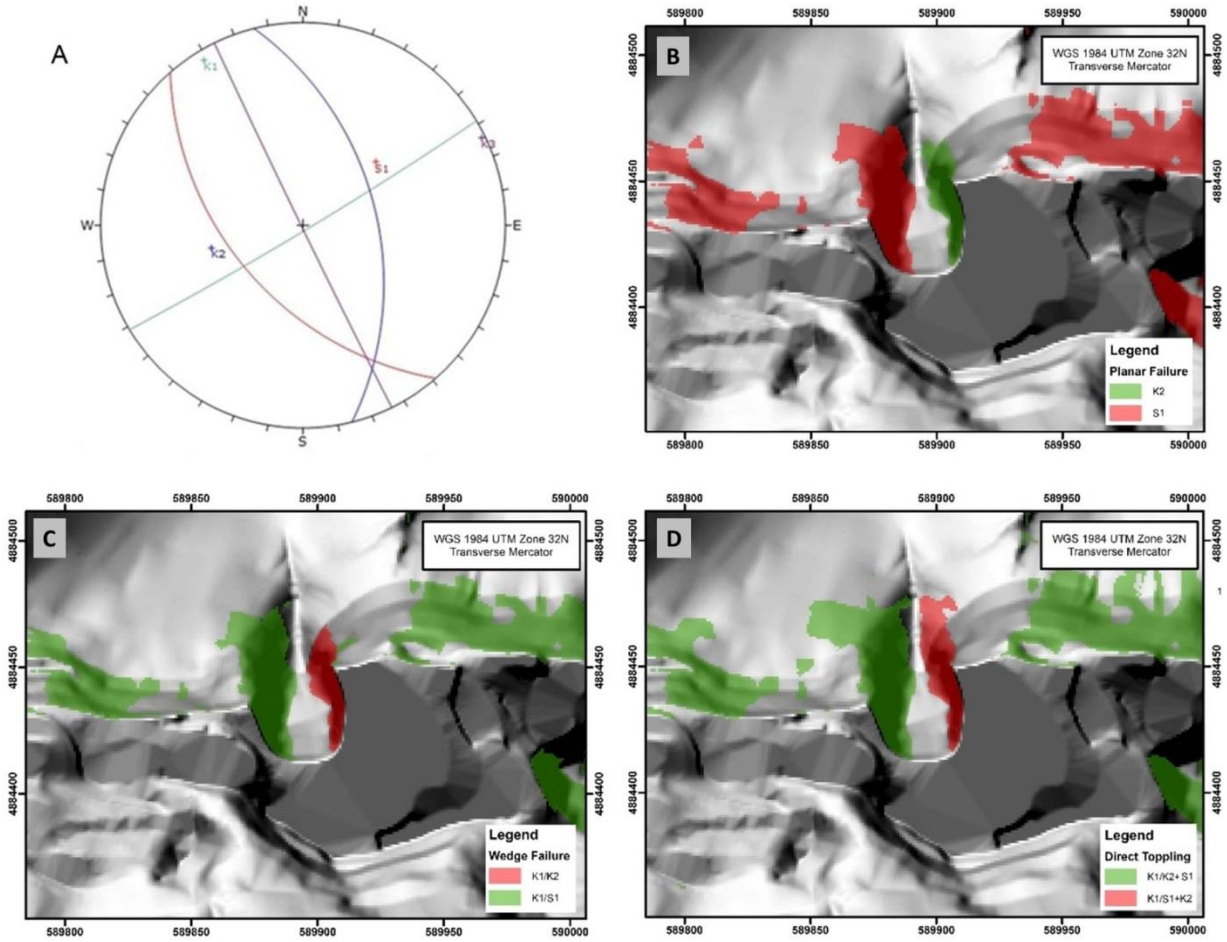

Figure 10. Results of the deterministic kinematic stability analysis: Stereographic representation of joint sets shown in Table 3 (A); areas potentially affected by planar failure (B); areas potentially affected by wedge failure (C); areas potentially affected by direct toppling (D).

Maps shown in Figures 10B and 10C highlight a strong similarity due to an important assumption in Rocscience™ [66] software regarding "pure" planar sliding on a single plane; in fact, in these types of analyses, the occurrence of release planes, such as lateral joints, or tension cracks is assumed to allow planar sliding. These planes are not explicitly involved in the conventional kinematic analysis for planar sliding, but it is important to be aware that a release mechanism must normally exist to allow removal of a block from the slope. This means that planar sliding can be considered as a special case of wedge failure where sliding takes place on only one plane, and other planes act as release planes. It should be noted that the foliation S1 was included in the analysis even if it is not a true open discontinuity set. This was undertaken to reflect the fact that the S1 foliation represents a direction of weakness in the rock mass which can have an important control on the dilation, nucleation and propagation of brittle fractures [18], [52] and [17]. This phenomenon is visible in the upper right of Figure 8 where low angle fractures (with irregular shape and direction similar to S1) seem to connect the high angle discontinuities that characterize the buttress face. For this reason, the authorities decided to leave in place wider benches at the base of the buttress with the aim to increase the overall stability and avoid the propagation of new generated fractures between system discontinuities.

6 Three dimensional stress analyses using the finite difference method, FLAC3D

DTP, TLS and the engineering geological surveys provide fundamental data for an improved understanding of the structural geological setting of the area. Using these methods it was possible to analyse whether the fractures on the slope were related to the complex geological history of the area and/or to the recent excavation activity. In fact, the progress of the excavation can cause the formation of new brittle fractures due to the unloading stress. Their existence in the Carrara marble district (called "*forzature*" by the local technicians) has been the cause not only of damage within the extracted blocks and slabs, but also of several rock fall events as documented by several authors; see e.g. [17] and [18]. In this research, the FLAC3D code [49] was used to analyse the stress distribution of the slope using the Finite Difference Method. Although FLAC is a continuum numerical modelling approach and is not appropriate to model a large number of fractures, selected discontinuities with simple intersections can be discretely included as interfaces [55]. Numerous authors have described the use of FLAC for the analysis of rock slopes and open pits [11], [43], [68].

6.1 Stress distribution using the induced lithostatic stress

In this study, Rhinoceros™ SR4 software [59] was used with the aim of creating a 3D model closely approximating the true geometry of the slope. TLS point clouds were processed to build the 3D model

and then exported into Kubrix software [49] to prepare for simulation using FLAC 3D [49]. Figure 11A-D shows the 3D model created by Rhinoceros™ SR4 and Kubrix. Figure 11A shows the initial geometry used to calculate the initial stress distribution. Figure 11B shows the reconstruction of the topography before the marble excavation. Figure 11C and D show the geometry of the buttress and the "history points" (points of interest) respectively; the latter were located at different elevations on the marble buttress and interrogated during the excavation progress.

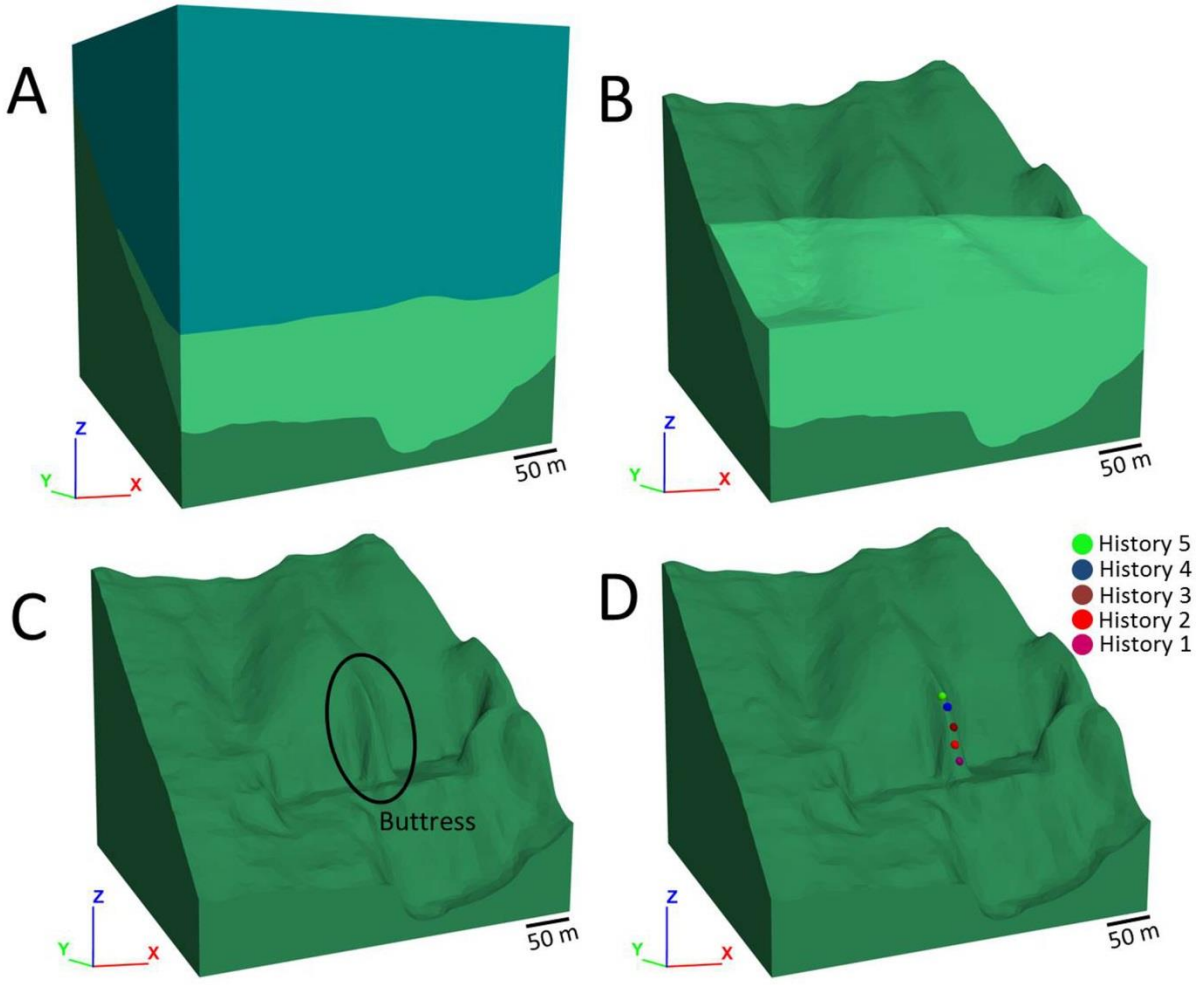

Figure 11. 3D model of the marble quarry and buttress created in Rhinoceros™ SR4 and Kubrix: Initial model (A), topography pre (B) and post (C) excavation and history points located in the buttress (D).

The marble was modelled as an elastic material with a unit weight of 27 KN/m^3 with joints not considered at this stage. The isotropic elastic and material option, in FLAC3D, provides the simplest representation

of material behaviour and is valid for homogeneous, isotropic, and continuous material that exhibits linear stress-strain behaviour.

This decision was made after a careful examination of the literature and that, given the strength of the marble rock mass and the limited depth of the quarry, little yield should occur under compressive stresses. Moreover, this decision was also taken in agreement with the studies carried out by Wiles [83]. Wiles, after a long discussion on the use and reliability of simple versus complex constitutive criteria noted that the use of an elasto-plastic model makes the calibration of the model extremely difficult due the uncertainty of the additional parameters required, (E, V and density vs E,v. Density, intact cohesion, intact friction, dilation, rock mass cohesion, rock mass friction). In essence at this stage in our models we have focused on location of stress concentrations, not yielding of these stresses. The latter would have necessitated the assumptions inherent in scale-dependent downgrading of the rock properties and hence possibly obscured the results. Wiles suggests, for making stress predictions, the use of an accurate geometry and simple model (Homogeneous, elastic modelling is the best option since the only significant parameter that must be specified is the far-field stress state). Table 5 shows the rock properties used in this first simulation (called "Analysis 1").

Parameters - Analysis 1	Value
Unit weight (KN/m^3)	27
Deformation modulus (GPa)	48
Poisson's ratio	0.27
Shear modulus (GPa)	19
Bulk modulus (GPa)	34

Table 5. Rock material parameters used in Analysis 1

Since the elevation of the model was approximately 440 meters, the lithostatic vertical stress σ_z (or σ_v) was estimated to be almost 12 MPa at the base of the model. This value was gradually decreased from the bottom to the top so that to be zero at the surface of the initial model. The K values, K_x and K_y in this preliminary analysis were assumed to be equal to 0.4 (Equations 1 and 2).

$K_x = \sigma_x / \sigma_z$ Equation 1

$K_y = \sigma_y / \sigma_z$ Equation 2

The deformation modulus was calculated using the GSI value and RocData 4.0 software (Rocscience™ 2014 and Hoek & Diederichs, 2006), while the Shear and Bulk moduli were calculated from equations 3 and 4:

$$G = E/2(1+\nu) \qquad \text{Equation 3}$$

$$K = E/3(1-2\nu) \qquad \text{Equation 4}$$

where G is Shear modulus, K the Bulk modulus and ν the Poisson's ratio.

The FLAC 3D code allowed the analysis of the stress distribution in the X, Y, and Z directions. Figure 12 shows the simulated stress distributions obtained in Analysis 1 in the X (Figure 12B), Y (Figure 12C), and Z (Figure 12D) directions respectively.

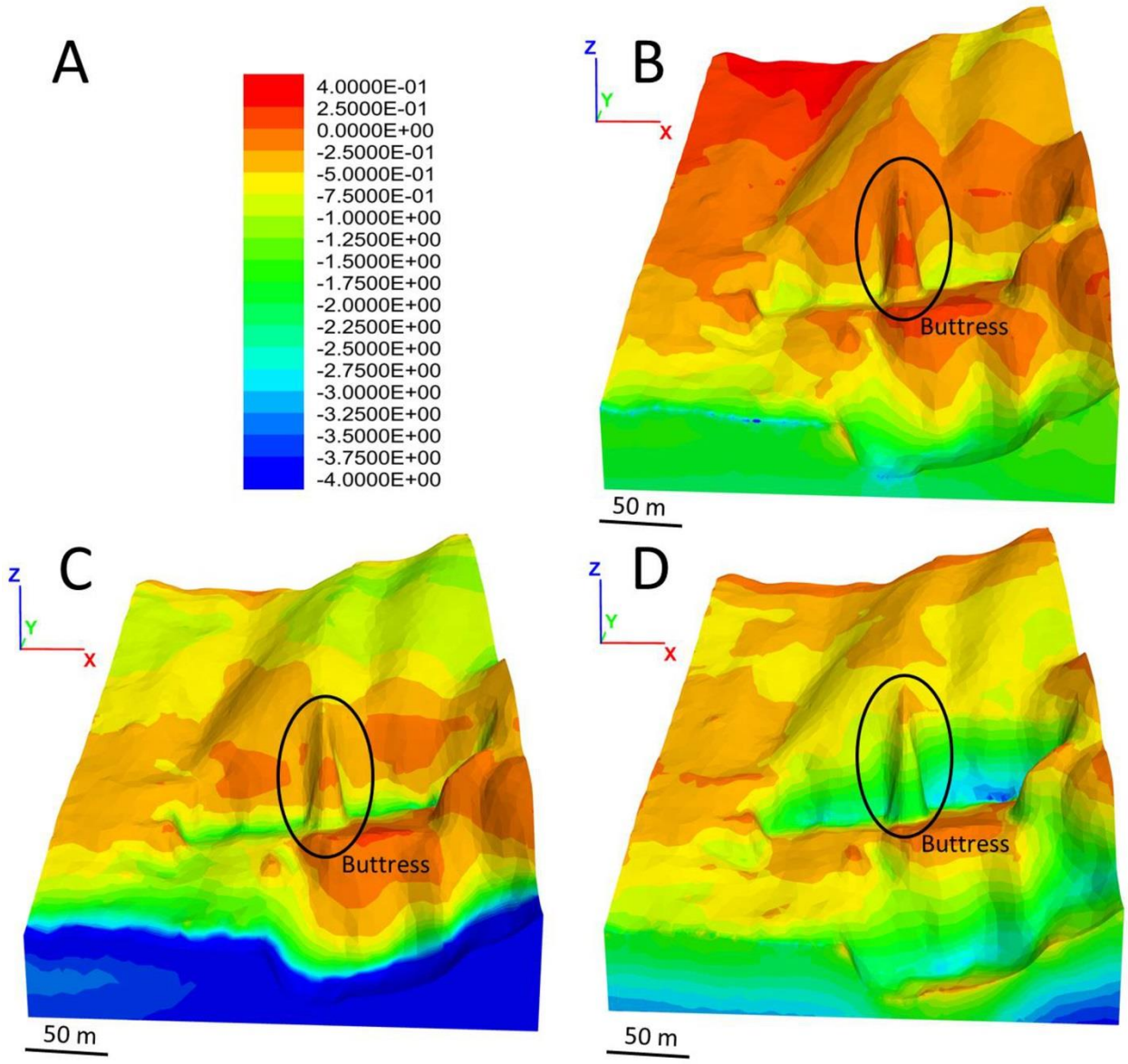

Figure 12. FLAC3D models for Analysis 1 showing the simulated stress distribution and magnitude; legend showing stress magnitude in MPa (A), stress distribution in XX direction (B), YY direction (C), and ZZ direction (D).

The stress values change from negative to positive indicating compressive and tensile stresses respectively. When positive values are present, the stress conditions are in tension and consequently, new fractures may be created, due to the unloading stress. Figure 12 shows positive tensile stress in the buttress with values in the X direction greater than in the Y direction. Figure 13 illustrates the stress state in the X and Y directions as measured at the history points (the x-axis represents the number of calculation steps in the analysis and the y-axis the value of stress in MPa).

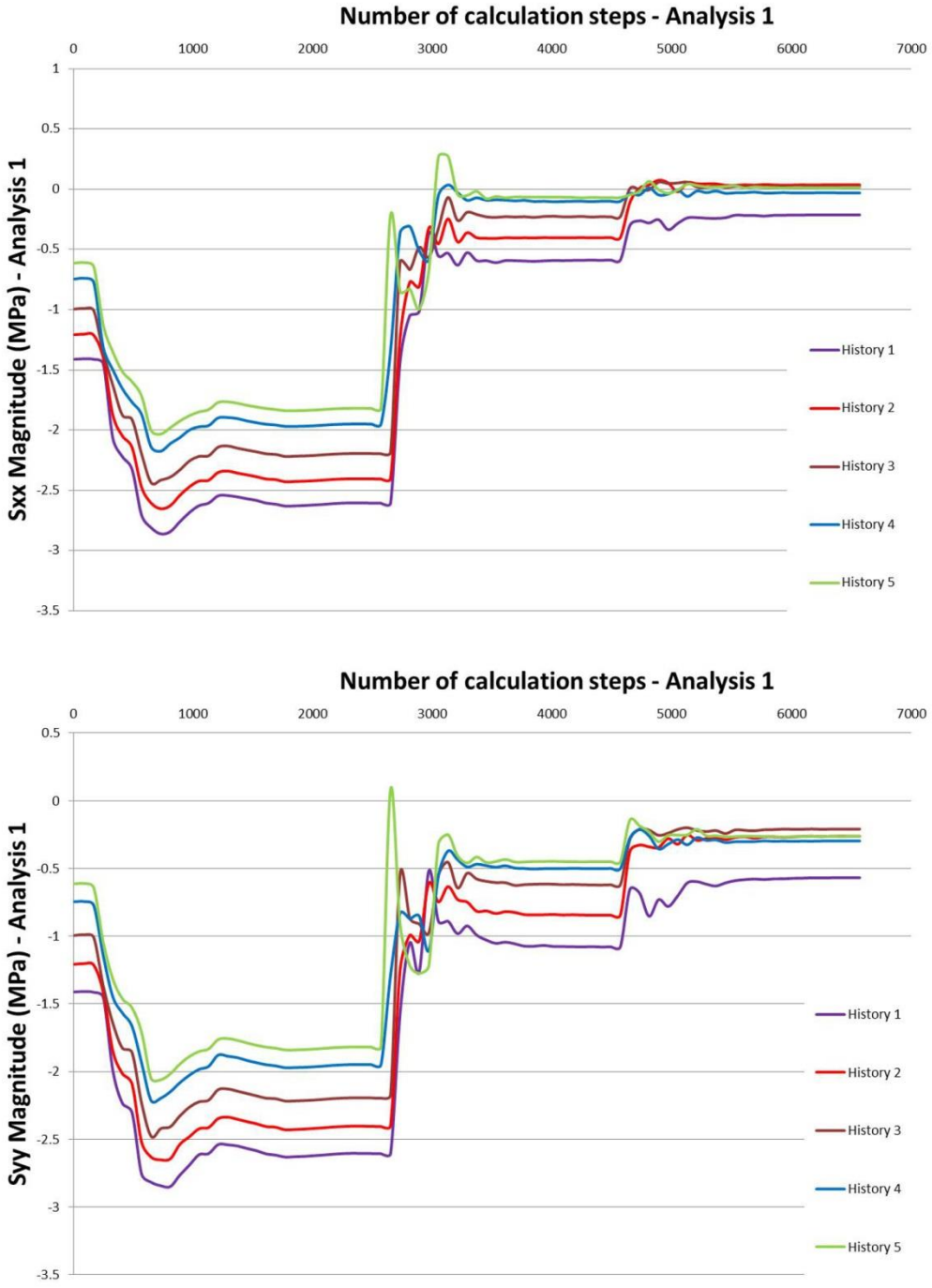

460

461 Figure 13. Analysis 1: simulated XX (top) and YY (bottom) stress magnitudes measured at the history

462 points, $K_x = K_y = 0.4$. Location of history points 1 to 5 shown in Figure 11D.

463

The graphs show how the X-stresses (SXX) reach positive values at history points number 2, 3 and 5 (up to 0.04 MPa at the history point 2) and how they have very low negative values (compressive) at history points 1 and 4. Moreover, all the history points show that Y-stresses (SYY) are very low and close to positive values but that tensile stresses are not observed. It is important to note that, owing to the lack of field in-situ stress measurements these results assume an initial $K_x=K_y$ value of 0.4 and do not take into account probable tectonic in-situ stresses; the results consequently show relative stress changes with excavation only and not the true absolute values.

In order to understand how the assumed in-situ stress ratio may influence the results of the study, further analyses were carried using different K_x, K_y values and stress tensors. The software WinTensor 4.0.4 [23] was used for this purpose.

6.2 Stress distribution analysis based on palaeostress tensor calculation and assumed K value

The main palaeostress tensor acting in the study area was estimated by the software WinTensor 4.0.4 using a stress inversion technique based on fault and joint measurements. The inversion is based on the assumption that slip on a plane occurs in the direction of the maximum resolved shear stress [18]. The data used for this process are the strike and dip of the fault planes, the orientation of the slip line and the sense of movement on the fault planes (which can be determined from grooves or slickensides). Data is inverted to obtain the characteristic parameters of the reduced palaeostress tensor according to Angelier and Mechler [5] and Delvaux [24]. The derived parameters refer to the attitude of the three principal stress axes σ_1, σ_2, σ_3 (where $\sigma_1 > \sigma_2 > \sigma_3$) and to the stress ratio R (Equation 5) which expresses the magnitude of the intermediate principal stress, σ_2 relative to the magnitude of the major and minor principal stresses σ_1 and σ_3 respectively. Some examples of the use of this software in the study of stress fields in different parts of the world are given in [59], [26], [24], [25], [76].

$$R = (\sigma_2 - \sigma_3) / (\sigma_1 - \sigma_3) \text{ with } 0 < R < 1 \qquad \text{Equation 5}$$

The analysis in WinTensor 4.0.4 was based on 20 measurements of kinematic indicators found on two different sides of the buttress and indicated two extensional regimes ($\sigma_1 = \sigma_v$) with two different stress tensors (Table 6). From the geological evidence visible in the area and in accordance with Bigazzi et al. [10], Carmignani and Kligfield [17] and Ottria and Molli [61], it is suggested that these two stress tensors are related to two different tectonic stages (so-called “D2S1” and “D2S2”) within the D2 tectonic phase. During the older stage (D2S1), strike-slip and extensional movements with a general East-West orientation took place at the same time (stress tensor 1 in Table 6). During the subsequent D2S2 further

tectonic denudation and unloading changed the deformation style toward a multi-directional extension which was probably North-South directed within the study area (stress tensor 2 in Table 6).

Stress Tensors	R	Type
1	0.5	Pure Extensional (nearly E-W orientation)
2	0.5	Pure Extensional (nearly N-S orientation)

Table 6. Stress tensors determined from analysis using WinTensor 4.0.4

Based on these results, two further FDM analyses (Analysis 2 and 3) were carried out simulating the latest extensional regime (North-South directed). As the Y axis corresponds, in this case, to the North-South direction, σ_y was set as the minor principal stress (σ_3) to reproduce the North-South directed extensional regime. The same lithostatic vertical stress σ_v, adopted in Analysis 1, was used and the K_x and K_y values were assumed as 0.6 and 0.4 respectively for Analysis 2 and 0.8 and 0.4 for Analysis 3.

Figures 14 and 15 show the results in terms of the simulated stress distribution in the X and Y directions for Analysis 2 (K_x = 0.6 and K_y = 0.4) and Analysis 3 (K_x = 0.8 and K_y = 0.4). Figures 16 and 17 show the simulated magnitude of stress values in Analysis 2 and 3 respectively at the same history points as used in Analysis 1. The two simulations confirm that positive (tensile) stress values can be reached in the buttress in the X direction (history points 2, 3, 4 and 5 for both Analysis 2 and 3). This agrees with field observations of the presence of visible stress-induced damage in the marble buttress noted during the engineering geological and photogrammetric surveys (Figure 8). Moreover, in these two analyses the magnitude of the tensile stresses are greater than obtained in Analysis 1(up to 0.15 MPa for the history point 2 in the analysis 2 and up to 0.2MPa for the same history point in Analysis 3).

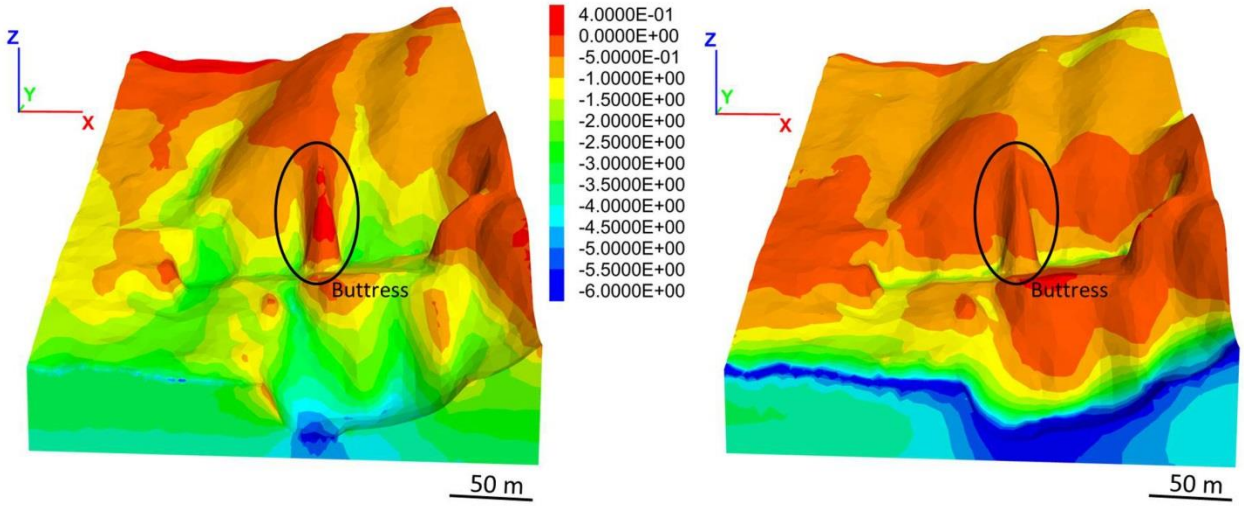

Figure 14: FLAC3D models for Analysis 2 showing the simulated stress distribution and magnitude; SXX stress distribution in X direction (left) and SYY stress distribution in Y direction (right), K_x = 0.6 and K_y = 0.4. Units of stress in MPa.

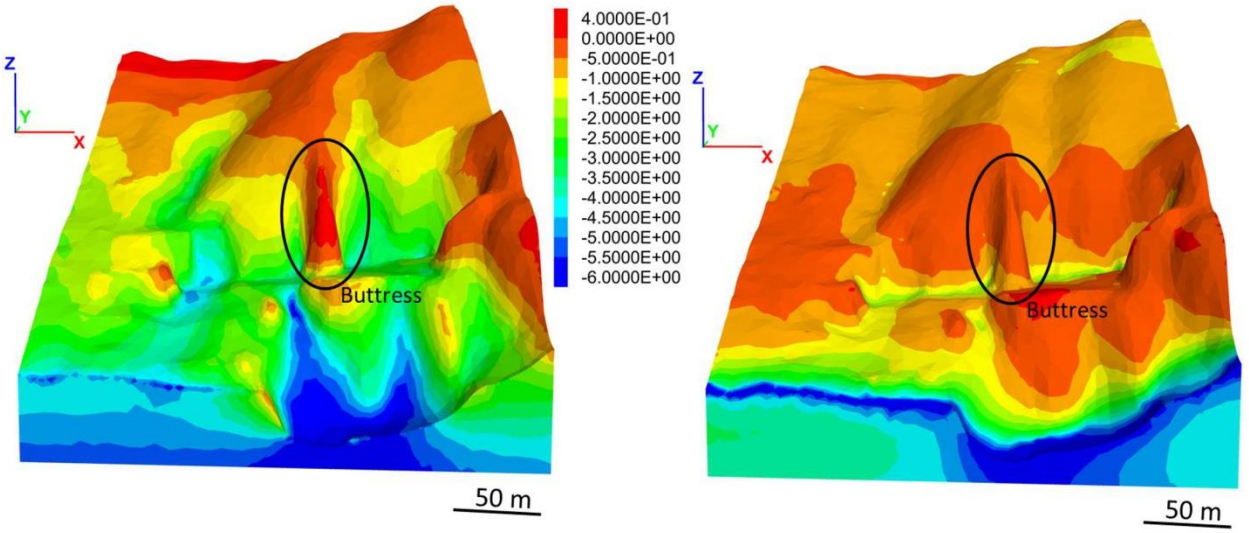

Figure 15: FLAC3D models for Analysis 3 showing the simulated stress distribution and magnitude; SXX stress distribution in X direction (left) and SYY stress distribution in Y direction (right), K_x = 0.8 and K_y = 0.4. Units of stress in MPa.

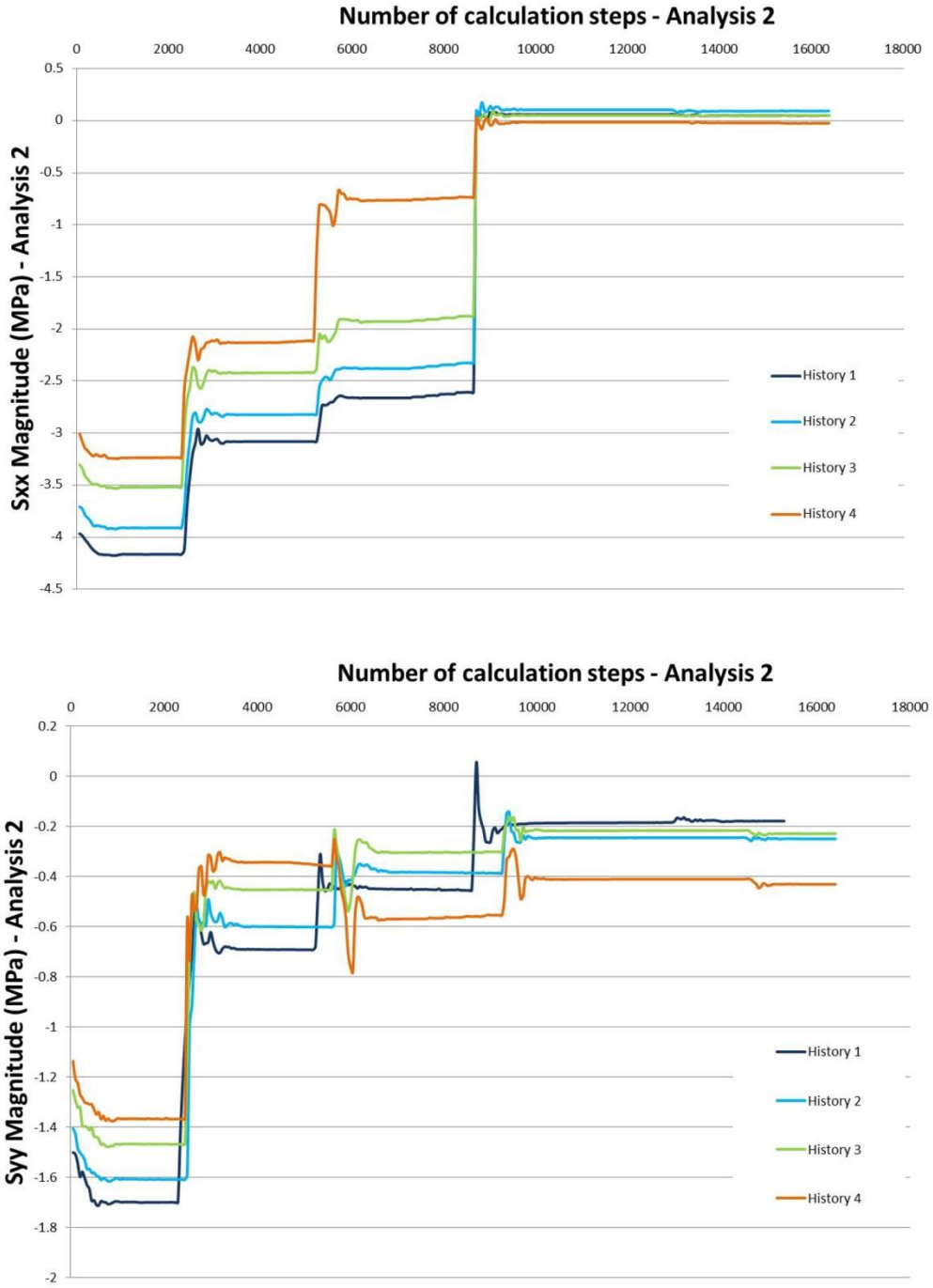

528

529 Figure 16. Analysis 2: simulated XX (top) and YY (bottom) stress magnitude measured at the history

530 points, $K_x = 0.6$ and $K_y = 0.4$. Location of history points 1 to 5 shown in Figure11D.

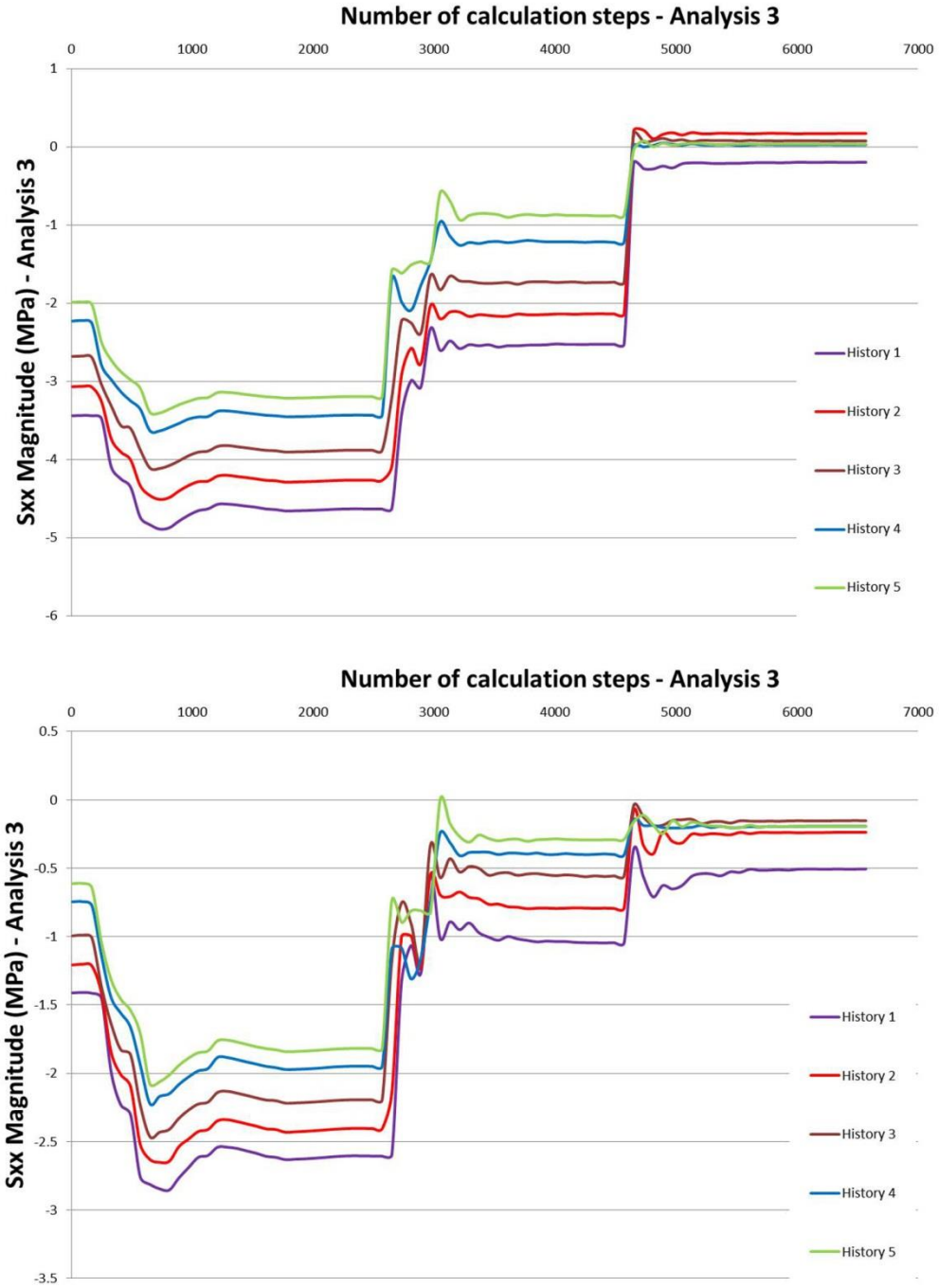

Figure 17. Analysis 3: simulated XX (top) and YY (bottom) stress magnitude measured at the history points, $K_x = 0.8$ and $K_y = 0.4$. Location of history points 1 to 5 shown in Figure11D.

7 Discussion

This research demonstrates how an integrated remote sensing - GIS approach can improve the overall understanding and the quality of data available for rock slope stability analysis. Recently, several DTP techniques have been used by various authors to demonstrate their potential advantages in conducting surveys in high and complex geometry rock slopes. Sturzenegger and Stead (2009a and b) showed how, with the use of a tripod and long range focal length camera lenses, it is possible to calculate the joint attitude with accuracies similar to those obtained from TLS. However, in case of complex rock slope geometry and where problems of inaccessibility are encountered, this system tends to leave shadow (occluded) areas in the output. Firpo et al. [33] and Francioni et al. [34] showed how the use of an aerostatic balloon can solve problems related to the complexity of the slope, however, the inaccessibility of the area facing the object under study can be an insurmountable problem. Salvini et al. [69] and [71], clearly illustrated how the use of a helicopter can overcome the above mentioned problems. The use of helicopter systems can be both complicated and expensive and the orientation of the photographs less precise when compared to conventional terrestrial methods of survey.

In this context, the advent of UAV systems represents a very important innovation for remote sensing techniques since it provides a very powerful and flexible tool for the acquisition of high resolution photographs. Moreover, they are remotely controlled, thus avoiding the need of a crew and their cost is highly variable and dependent on the specific site requirements. The use of UAV technology in the earth sciences and more specifically in engineering geology has been documented in the literature [42], [60]. In this research the survey was executed using a vehicle that can work in an autonomous manner or be managed from the ground by remote control. Using this vehicle, it was possible to survey both the open pit surface, which is characterized by a very steep geometry, and an overhanging slope which has a complex morphology. All the photographs acquired by the UAV were oriented through the integrated use of TS and differential GPS surveys. This procedure provides a very powerful approach for increasing precision and accuracy of the photograph orientation and TLS registration procedures. The errors obtained during the exterior orientation of photographs, shown in Table 2, are considered acceptable given the survey distance and the complexity of the slope morphology. In fact, in spite of the accuracy obtained in the measurement of GCP by topographic survey, the UAV is a light and remotely controlled vehicle which can be prone to vibrations and instability phenomena during photograph acquisition. These problems can result in misalignment of photographs and significant errors during their orientation. Recently, the acquisition of a large number of photographs and the use of powerful software including image matching algorithms for the orientation process and the creation of DSM and orthophotos (see Agisoft™ Photoscan Professional [1]) has been shown to decrease these errors. However, if the attitude of

571 the UAV is properly controlled, the orientation of photographs permits the creation of accurate
572 stereoscopic models and the stereo-restitution and measurement of geological features such as joint
573 attitude, spacing, and trace length.
574 TLS was used in this research to obtain a very high resolution 3D model of the slope and to validate the
575 results obtained from the stereo-restitution. Three different point clouds were acquired to avoid occlusions
576 at the rock slope face and subsequently registered to a unique model thanks to the topographic survey.
577 The maximum error estimated during the registration process was approximately 5 mm which is
578 considered to be acceptable. Joint sets derived from DTP and TLS were compared (Figure 5) and show a
579 good agreement in terms of both mean dip and dip directions.
580 To complement the geomatic surveys, engineering geological surveys were carried out to provide
581 supplementary information on the physical-mechanical characteristics of the joints and the rock mass.
582 Data obtained from these surveys was used in the characterization of rock mass according to the
583 Bieniawski RMR method and for estimation of the GSI. The values of RMR and GSI made it possible to
584 classify the rock mass as "good" in accordance with previous studies [63]. It must be highlighted that the
585 engineering geological survey permitted the definition of the joint sets recognizable at the base of the
586 open pit only and, consequently it is possible to observe some differences between the values obtained
587 from DTP and TLS.
588 In addition, a kinematic analysis was carried out in order to analyse the stability of the buttress and the
589 overhanging natural slope. Considering the quality and the amount of data available from the above
590 mentioned surveys, this analysis was performed using a deterministic approach. The study area was
591 subdivided into different zones based on a spatial analysis carried out by GIS techniques. The results
592 obtained from this analysis are in agreement with previous studies carried out in the area by geologists
593 and professional hand scaling personnel and with the mitigation work previously carried on the slope
594 [63].
595 The last component of this research was a FDM analysis of the stress distribution in the buttress broadly
596 representative of its geological history and recent excavation stages. It is known from literature how
597 stress-induced damage due to excavation is a frequent problem in mining and quarrying activities and, as
598 mentioned previously, the presence of such stress-induced fractures was found in the study area. These
599 newly generated stress-induced brittle fractures may be an important consideration in the stability of an
600 area and their study could decrease the risk of failure and increase the quality of marble in future
601 extraction works. For this reason, with the aim of improving knowledge of the stress distribution in the
602 marble buttress, FDM analyses were carried out using FLAC 3D. An initial analysis (Analysis 1) was
603 performed using the induced lithostatic stress and K_x and K_y values both equal to 0.4. The simulation

results showed positive tensile stresses in certain positions on the buttress. Numerous researchers have recently noted the role of tensile damage on rock slopes [28], [14], [15], [74] [75].

It is important to emphasise that the concentration of tensile stresses may be increased if high in-situ tectonic stresses are present. Since in-situ measurements regarding actual tectonic in-situ stress are not available, it was decided to use the WinTensor software in an attempt to investigate the most probable main stress tensors in the area. The study of palaeostress carried out with the WinTensor software helps to understand how structures influenced the geological history of the area (e.g. based on the Anderson's classification – Anderson, [2]). It should be emphasised however the direction of palaeostress does not necessarily coincide with the current stress tensor acting today. Nevertheless, recent studies carried out in the Carrara marble district have confirmed that in this area there is a good correspondence between palaeostress data gained with WinTensor and the stress acting today [61], [48] [41], [31].

The analysis described in this paper has highlighted the presence of two main stress tensors: the first East-West directed and the second North-South. This result agrees with the theory that two different tectonic stages (D2S1 and D2S2) took place within the D2 phase [10], [17], [61]. Two further FDM analyses was then carried out (Analysis 2 and 3) simulating the most recent extensional regime (North-South directed) and using K_x and K_y values equal to 0.6 and 0.4 for the Analysis 2 and to 0.8 and 0.4 for the Analysis 3 respectively. From the results of the FLAC3D simulation, it was possible to show how a relatively small change in in situ stress ratio, K, modifies the spatial stress distribution. In fact, when comparing the results of Analysis 1, 2 and 3, it is notable how in Analyses 2 and 3 the stress values measured in the X direction at history points 2, 3, 5 and 5 attain positive (tensile) values and how these values increase going from Analysis 1 to 3. This agrees with field observations of the presence of visible stress-induced damage in the marble buttress noted during the engineering geological and photogrammetric surveys.

It should be emphasised that the WinTensor analysis is based on only 20 measurements due to the difficulty in finding more slickenside kinematic indicators within the area (due to erosion and inaccessibility). For this reason and because of the major importance that direct measurement of stress can have on future slope analyses, it is clear that the described WinTensor stress study represents a first preliminary stage in improving the understanding of the in-situ stress acting in the area and that further in-situ measurements would be necessary to better clarify stress response and induced damage within the marble buttress.

8. Conclusions

In this research an integrated remote sensing - GIS approach was used to improve the overall understanding and the quality of data available for the analysis of the Lorano open pit. The methodology

638 described overcomes a frequent problem related to the inaccessibility of rock slopes, owing to their
639 height, which can lead to erroneous evaluations of stability. DTP and TLS are shown to provide powerful
640 modelling and analytical tools in the study of the geometry of the slope. DTP was carried out through the
641 use of a UAV system. This technique overcomes problems related to elevation, steepness and complex
642 geometry of slope; it is less expensive than other photogrammetric techniques showed in previous
643 research such as aerostatic balloons and helicopters and with a good flight plan photogrammetric
644 acquisition of areas can be obtained that would be impossible to survey with any other vehicle or
645 methodology. TLS was performed using a long range laser scanner (up to 1 Km range) with three
646 different point clouds acquired to avoid occlusions. The TLS model was overlapped with the
647 photogrammetric model to create a high resolution 3D model useful in the definition of the main
648 geological features and in the development of the 3D slope model to be used in subsequent kinematic and
649 numerical analysis.
650 Kinematic analysis was carried out using GIS techniques. Using developed thematic maps, different
651 kinematic analyses were performed according to the varying slope geometries so as to determine the
652 steepest safe angles. As a result, this approach was able to overcome the common problem of complex
653 slope geometry encountered in kinematic slope analyses.
654 Finally, a FDM analysis of the stress distribution in the buttress was performed to verify the possibility of
655 tensile stress generation after the excavation phase. A study of palaeostress was carried out with the
656 WinTensor software to understand how structures influenced the geological history of the area. Based on
657 this study, a sensitivity analysis using different K values was performed in FLAC 3D to evaluate the
658 influence of assumed in-situ stress ratio on the simulated stress distribution in the buttress. This research
659 demonstrates that unloading due to erosion and slope excavation can lead to tensile stress in the marble
660 buttress and that this will be amplified when high in-situ stress conditions are present. The FDM
661 simulation shows that, even though the tensile stresses do not reach very high magnitudes and they might
662 not be enough to generate brittle fractures in the intact rock mass (for the Kx and Ky values until now
663 investigated), they are parallel to the X direction (West-East) which is approximately the same direction
664 as the strike of the S1 foliation surfaces that characterize most of the Apuan Alps. As the S1 foliation
665 represents the direction of weakness in the rock mass, it is suggested that S1 may have an important
666 control on the nucleation and propagation of brittle fracturing. Moreover, as before mentioned, the new
667 generated fractures, was observed connecting two adjacent system discontinuities.
668 This agrees with the field observations (often the brittle fractures in the Carrara marble district follow the
669 same direction as S1) and previous studies carried out in the area [18], [52] and [17]. Although this
670 research represents a preliminary study, it forms an important step and foundation for the analysis of the

671 buttress and a case example of stress analysis/damage in open pit slopes using a remote sensing/FDM
672 approach.
673
674 *8.1 Future developments and works*
675 Field measurements of in-situ stress were not available for this research. As this data becomes available
676 (in collaboration with the *Unità Sanitaria Locale* - USL1 of Massa-Carrara), further numerical modelling
677 will be carried out to allow the absolute stress distribution during the quarry excavation phases to be
678 better understood (particularly in order to evaluate the buttress behaviour in case of low and very low (up
679 to ≈ 0,1) Kx and Ky values [32].
680 Laboratory testing will be performed to improve the information on the mechanical properties of the
681 marble and to better define the role of the S1 foliation in the tensile strength of the rock. Further
682 numerical simulation will then also be undertaken using a FDEM-DFN (Discrete fracture Network)
683 approach (e.g. Elfen and Slope Model [65] [49]) to allow simulation of stress-induced brittle fracture
684 generation and propagation. Based on the research presented in this paper further protection works were
685 carried out on the natural slope overhanging the open pit and three different monitoring systems installed
686 which have been operational since 2012 [72]. The first is a geotechnical monitoring system comprising
687 extensometers and crack-meters, and the other two are topographic systems consisting of a terrestrial
688 interferometer and a robotic total station. Data from these instrumentation systems will form an important
689 constrain for future rock slope damage research and constraining existing and future stability models of
690 the buttress area.
691
692 **Acknowledgments**
693
694 The authors wish to thank the Carrara USL1 (Mining Engineering Operative Unit – Department of
695 Prevention in the person of Eng. Pellegri, M.), La Sapienza University of Rome (Prof. Bozzano, F. leader
696 of the Italian National Research Project PRIN2009), and Ingeo Systems – Leica Geosystems (Eng.
697 Lapini, M.). Moreover, we are extremely grateful to the company "Cooperativa Cavatori Lorano" and, in
698 particular, to the quarry manager Ferrari, M.
699
700 **References**
701 [1] Agisoft™ Photoscan Professional, 2014. http://www.agisoft.ru/products/photoscan.
702 [2] Anderson, E. M. 1951. The Dynamics of Faulting and Dyke Formation with Application to
703 Britain. Oliver and Boyd, Edinburgh, ed. 2:206.

[3] Abellán, A., Vilaplana, J.M., Martinez, J. 2006. Application of a long-range Terrestrial Laser Scanner to a detailed rock fall study at Vall de Núria (Eastern Pyrenees, Spain). Engineering Geology 88, 136-148.

[4] Alvafez, W., Cocozza T., Wezel, F.C. 1974. Fragmentation of the Alpine orogenic belt by microplate dispersal. Nature 248, 309-314.

[5] Angelier, J., Mechler, P. 1977. Sur une methode graphique de recherche des contraintes principales egalement utilisable en tectonique et en seismologie: 1a methode des diedres droits, Bull. Soc. Geol. France, 7(19), 1309-1318.

[6] Aringoli, D. Calista, M., Gentili, B., Pambianchi, G., Sciarra, N. 2008. Geomorphological features and 3Dmodelling of Montelparo mass movement (Central Italy), Engineering Geology, 99, 70-84.

[7] Beraldin, J. A. 2004. Integration of laser scanning and close-range photogrammetry— the last decade and beyond. Proceedings: XXth International Society for Photogrammetry and Remote Sensing (ISPRS) Congress, Istanbul, Turkey, 972-983.

[8] Bieniawski, Z. 1973. Engineering classification jointed rock masses. Transactions of the South African Institution of Civil Engineers, 15, 335-344.

[9] Bieniawski, Z. 1989. Engineering Rock Masses Classification. John Wiley and Sons Inc. New York, NY, USA, 272 pp.

[10] Bigazzi, G., di Pisa, A.,Gattiglio, M., Meccheri, M., Norelli, P. 1988. La struttura catoclastica-milonitica di Foce di Mosceta, Alpi Apuane sud orientali (M. Corchia, Gruppo delle Panie). Atti Soc Sci. Nat., Mem. Ser. A., 95, 105-116.

[11] Board, M., Chacon, E., Varona, P., Lorig, L. 1996. Comparative analysis of toppling behaviour at Chuquicamata open-pit mine, Chile. Trans. Instit. Min. Metall., 105, A11-A21.

[12] Bott, M.H.P. 1959. The mechanisms of oblique slip faulting. Geol. Mag. 96. 109-117.

[13] Brideau M.A., Pedrazzini A., Stead D., Froese C., Jaboyedoff M., van Zeyl D. 2011. Three-dimensional slope stability analysis of South Peak, Crowsnest Pass, Alberta, Canada. Landslides, 8, 139-158.

[14] Cai, M., Kaiser, P.K., Martin, C.D. 2001. Quantification of rock mass damage in underground excavations from microseismic event monitoring, International Journal of Rock Mechanics and Mining Sciences, 38, 1135-1145.

[15] Cai, M., Kaiser, P.K., Tasaka, Y., Maejima, T., Morioka, H., Minami. M. 2004. Generalized crack initiation and crack damage stress thresholds of brittle rock masses near underground excavations. International Journal of Rock Mechanics and Mining Sciences, 41, 833-847.

737 [16] Cai, M., Kaiser, P.K., Morioka, H., Minami, M., Maejima, T., Tasaka, Y., Kurose, H. 2007.
738 FLAC/PFC coupled numerical simulation of AE in large-scale underground excavations. International
739 Journal of Rock Mechanics and Mining Sciences, 44, 550-564.
740 [17] Carmignani, L., Kligfield, R, 1990. Crustal extension in the Northern Apennines: the transition
741 from compression to extension in the Alpi Apuane core complex. Tectonics, v9,1275-1303.
742 [18] Carmignani, L.,Conti, P., Fantozzi, P.L., Mancini S., Massa G., Molli G., Vaselli L. 2007. I
743 marmi delle Alpi Apuane. Geoitalia; 21, 19-30.
744 [19] Chang C.T., Monteiro P., Nemati K., Shyu K. 1996. Behavior of marble under compression.
745 Journal of Materials in Civil Engineering, Vol. 8, No. 3, August 1996, pp. 157-170.
746 [20] Coggan, J.S., Wetherelt, A., Gwynn, X.P., Flynn, Z. 2007. Comparison of hand-mapping with
747 remote data capture systems for effective rock mass characterisation, 11th Congress of International
748 Society for Rock Mechanics, Lisbon 2007, 9th - 13th July 2007, Proceedings of 11th Congress of the
749 International Society for Rock Mechanics - the second half century of rock mechanics, 1, 201-205.
750 [21] Cruden, D.M. 1989. Limit to common toppling. Can Geotech J 26:737-742
751 [22] Danzi, M., Di Crescenzo, G., Ramondini, M., Santo, A. 2013. Use of unmanned aerial vehicles
752 (UAVs) for photogrammetric surveys in rockfall instability studies. Rendiconti Online Societa Geologica
753 Italiana, 24, 82-85
754 [23] Dahal, R.K., Hasegawa, S., Nonomura, A., Yamanaka, M., Dhakal, S. 2008. DEM-based
755 deterministic landslide hazard analysis in the Lesser Himalaya of Nepal, Georisk 2, 161-178.
756 [24] Delvaux, D. 1993. Quaternary stress evolution in East Africa from data of the western branch of
757 the East African rift. In: Thorweihe, Schandelmeier (Eds.), Geoscientific Research in Northern Africa,
758 Balkema, Rotterdam, pp. 315-318.
759 [25] Delvaux, D., Barth, A. 2010. African stress pattern from formal inversion of focal mechanism
760 data. Implications for rifting dynamics. Tectonophysics 482, 105-128.
761 [26] Delvaux, D., Kervyn, F., Macheyeki, A., Temu, E.B. 2012. Geodynamic significance of the TRM
762 segment in the East African Rift (W-Tanzania): Active tectonics and paleostress in the Ufipa plateau and
763 Rukwa basin, Journal of Structural Geology, 37, 161-180.
764 [27] Delvaux, D. Sperner, B. 2003. Stress tensor inversion from fault kinematic indicators and focal
765 mechanism data: the TENSOR program. In: New Insights into Structural Interpretation and Modelling (D.
766 Nieuwland Ed.). Geological Society, London, Special Publications, 212: 75-100.
767 [28] Diederichs, M.S., 1999. Instability of hard rock masses: the role of tensile damage and relaxation.
768 PhD thesis, University of Waterloo.

769 [29] Diederichs, M.S, Kaiser, P.K., Eberhardt, E. 2004. Damage initiation and propagation in hard
770 rock during tunnelling and the influence of near-face stress rotation. International Journal of Rock
771 Mechanics and Mining Sciences, 41, 785-812.
772 [30] Feng, Q.H., Röshoff, K., 2004. In-situ mapping and documentation of rock faces using a full-
773 coverage 3D laser scanner technique. International Journal of Rock Mechanics and Mining Sciences 41
774 (3), 139-144.
775 [31] Ferrero, A. M., Forlani G., Rondella R., Voyat H.I. 2009. Advanced geostructural survey methods
776 applied to rock mass characterization. Rock Mech Rock Eng 42 (4), 631-65.
777 [32] Ferrero A.M., Gullì D., Migliazza M., Segalini A. 2013. In situ stress measurements
778 interpretations in large underground marble quarry by 3D modeling. International Journal of Rock
779 Mechanics and Mining Sciences, Vol. 60, pp. 103-113.
780 [33] Firpo, G., Salvini, R., Francioni, M., Ranjith, P.G. 2011. Use of Digital Terrestrial
781 Photogrammetry in rock slope stability analysis by Distinct Element numerical methods. International
782 Journal of Rock Mechanics and Mining Science, 48 (7), 1045-1054.
783 [34] Francioni. M., Salvini, R., Stead, D. Litrico, S. 2014. A case study integrating remote sensing and
784 distinct element analysis to quarry slope stability assessment in the Monte Altissimo area, Italy.
785 Engineering Geology, 183, 290-302.
786 [35] Francioni M. 2013. Development in the study of rock slopes: an integrated remote sensing –
787 stability analysis approach. PhD thesis. University of Siena.
788 [36] Francioni, M, Girgenti C. and Vanneschi C. 2013. Underground quarrying industry and terrestrial
789 laser scanning. Proceedings to IX Convegno Giovani Ricercatori di Geologia Applicata. Napoli, Italy,
790 14th - 15th February 2013.
791 [37] Fröhlich, C., Mettenleiter, M. 2004. Terrestrial laser scanning — new perspectives in 3D
792 surveying. In: Thies, M., Koch, B., Spiecker, H., Weinacker, H. (Eds.), Laser-scanners for Forest and
793 Landscape
794 [38] Ghirotti, M., Genevois, R. 2007. A complex rock slope failure investigated by means of
795 numerical modelling based on laser scanner technique. In Proceedings: 1st Canada-US Rock Mechanics
796 Symposium, Eds E, Eberhardt, D. Stead and T. Morrison, May 27-31, Vancouver, 917-924.
797 [39] Goodman, R.E. 1989. Introduction to rock mechanics, 2nd edn. Wiley, New York, p 576
798 [40] Goodman, R.E., Bray, J.W. 1976. Toppling of rock slopes. In: Rock engineering for foundations
799 and slopes, Proceedings of a Specialty Conference vol. 2. American Society of Civil Engineering, New
800 York, p. 201-234.

[41] Gullì, D., Pellegri, M., Cortopassi, A. 2010. Experimental study for stress analysis on different Carrara marble underground quarries. International Symposium on Deformation Characteristics of Geomaterials, September 1-3, Seoul, Korea, 1296 - 1302.

[42] Haarbrink, R.B., Eisenbeiss, H. 2008. Accurate DSM production from unmanned helicopter systems. International Archives of Photogrammetry, Remote Sensing and Spatial Information Sciences, XXXVII/B1. PRC, Beijing, 159-164.

[43] Handley, M. F., Karparov, K. N. 2007. Proposed thrust failure analytical method for slope collapse in open pit mines," in The Second Half Century of Rock Mechanics (11th Congress of the International Society for Rock Mechanics, Lisbon, July 2007), Vol. 1, pp. 645-652, L. Ribeiro e Sousa, C. Olalla, and N. Grossmann, Eds. London: Taylor & Francis Group.

[44] Haneberg, W.C. 2008. Using close range terrestrial digital photogrammetry for 3-D rock slope modelling and discontinuity mapping in the United States. Bulletin of Engineering Geology and the Environment, 67: 457-469.

[45] Hoek, E., Brown, E.T. 1997. Practical estimates of rock mass strength. International Journal of Rock Mechanics and Mining Sciences 34 (8), 1165-1186.

[46] Hoek, E., Bray, J.W. 1981. Rock slope engineering, Third edition. The Institution of Mining and Metallurgy, London, 358 pp.

[47] Hoek, E., Diederichs, M.S. 2006. Empirical estimation of rock mass modulus. International Journal of Rock Mechanics and Mining Sciences 43 (2), 203-215.

[48] Iabichino, G., Gullì, D., Cravero M., Bianchini, S. 2006. Comparison between 2D overcoring and hydraulic fracturing stress measurements in the Apuane Alps. In-situ Rock Stress – Lu, Li, Kjørholt & Dahle (eds) Taylor & Francis Group, London, ISBN 0-415-40163-1

[49] Itasca Software 2012. FLAC3D; Kubrix; Slope Model. http://www.itascacg.com/software/flac3d

[50] Jaboyedoff M, Baillifard F, Couture R, Locat J, Locat P. 2004. Toward preliminary hazard assessment using DEM topographic analysis and simple mechanic modeling. In: Lacerda WA, Ehrlich M, Fontoura AB, Sayo A (eds) Proceedings of the 9th International symposium on landslides. Balkema, Rotterdam, pp 191-197

[51] Jaboyedoff, M., Oppikofer, T., Minoia, R., Locat, J., Turmel, D. 2008. Terrestrial LIDAR investigation of the 2004 rockslide along Petit Champlain Street, Québec City (Québec, Canada). Proceedings: 4th Canadian Conference on Geohazards, 20-24May, Québec, Canada, 8 pp.

[52] Kligfield, R. 1979. The Northern Apennines as a collisional orogeny. Am. J. Sci. 279, 676-69.

[53] Kraus, K. 2007. Photogrammetry, Geometry from Images and Laser Scans. Berlin: De Gruyter.

[54] Lato, M., Diederichs, M.S., Hutchinson, D.J., Harrap, R. 2009. Optimization of LiDAR scanning and processing for automated structural evaluation of discontinuities in rock masses. International Journal of Rock Mechanics and Mining Sciences 46, 194-199.

[55] Lightfoot, N., Maccelari, M.J. 1999. Numerical Modelling of Mine Workings. SIMRAC Final Project Report GAP 415. Pretoria: Department of Minerals and Energy.

[56] Linder, W., 2003. Digital Photogrammetry - Theory and Applications. Heidelberg.

[57] Marinos, V., Marinos, P., Hoek E, 2005. The geological strength index: applications and limitations. Bull Eng Geol Environ 64:55-65.

[58] Maurenbrecher P.M., Hack H.R.G.K. 2007. Toppling mechanism: resolving the question of alignment of slope and discontinuities. In: Ribeiro e Sousa L, Ollala C, Grossmann N, (eds) 11th Congress of the International Society for Rock Mechanics. Taylor and Francis, London, pp 725-728.

[59] McNeel and Associates, 2011. Rhinoceros 4, SR9. http://www.rhino3d.com/download/rhino/4.0.

[60] Niethammer, U., Rothmund S., James M. R., Travelletti J., Joswig M. 2010. UAV-based remote sensing of landslides. International Archives of Photogrammetry, Remote Sensing and Spatial Information Sciences, Vol. XXXVIII, 496 - 501.

[61] Ottria G., Molli G. 2000. Superimposed brittle structures in the late-orogenic extension of the northern Apennine: results from the Carrara area (Alpi Apuane, NW Tuscany). Terra Nova, Vol. 12, 52-59.

[62] Perazzelli P., Graziani A., Rotonda T. 2009. Stability analysis of an active marble quarry by DEM modelling. Proceedings of the International Conference on Rock Joints and Jointed Rock Masses, Arizona, USA, January 7-8, 2009.

[63] Profeti, M., Cella, R. 2010. Relazione sulla stabilità dei fronti – Cava Lorano n. 22. Technical report.

[64] Richards, L.R., Leg, G.M.M., Whittle, R.A. 1978. Appraisal of stability conditions in rock slopes. In: Bell FG (ed) Foundation engineering in difficult ground. Newnes-Butterworths, London, pp 449-512.

[65] Rockfield 2012. ELFEN 2D/3D Numerical Modelling Package. Rockfield Software Ltd., Swansea. http://www.rockfield.co.uk/

[66] Rocscience 2014. Rocscience software products - DIPS 6.0, RocData 5.0. https://www.rocscience.com.

[67] Roncella, R., Forlani, G., Remondino, F. 2005. Photogrammetry for geological applications: automatic retrieval of discontinuity orientation in rock slopes. In: Proc SPIE-IS&T electronic imaging, Videometrics 5665,17-27.

[68] Sainsbury, B., Pierce, M. Mas Ivars, D. 2008. Analysis of Caving Behavior Using a Synthetic Rock Mass - Ubiquitous Joint Rock Mass Modeling Technique, In Proceedings of the 1st Southern

867 Hemisphere International Rock Mechanics Symposium (SHIRMS), Y. Potvin, J. Carter, A. Dyskin and R.
868 Jeffrey (eds), 16 - 19 September 2009, Perth, Australia, Australian Centre for Geo-mechanics, Perth, Vol.
869 1 - Mining and Civil, pp. 243 - 254.
870 [69] Salvini, R., Francioni, M., Fantozzi, P.L., Riccucci, S., Bonciani, F., Mancini, S. 2011. Stability
871 analysis of "Grotta delle Felci" Cliff (Capri Island, Italy): structural, engineering-geological,
872 photogrammetric surveys and laser scanning. Bull. Eng Geol Environ 70, 549-557.
873 [70] Salvini, R., Francioni, M. 2013. Geomatic for slope stability and rock fall runout analysis: a case
874 study along the Alta Tambura road in the Apuan Alps (Tuscany, Italy). Italian Journal of Engineering
875 Geology and Environment. Book series 6, Genevois R and Prestininzi A. (eds.), 481-492.
876 [71] Salvini, R., Francioni, M., Riccucci, S., Bonciani, F., Callegari, I. 2013. Photogrammetry and
877 laser scanning for analyzing slope stability and rock fall runout along the Domodossola–Iselle railway,
878 the Italian Alps. Geomorphology 185, 110-122.
879 [72] Salvini R., Vanneschi C., Gullì D., Forchione F., Riccucci S. and Francioni M. 2014. Integration
880 of geotechnical and remote monitoring systems for the analysis and control of ground deformation in
881 marble quarrying (Apuan Alps, Italy). in "Engineering Geology for Society and Territory. Vol. 5 Urban
882 Geology, Sustainable Planning and Landscape Exploitation", Lollino G., Manconi A., Guzzetti F.,
883 Culshaw M., Bobrowsky P. and Luino F. (eds.), 183-188.
884 [73] Slama, C.C. (Ed.) 1980. Manual of Photogrammetry, 4th edition. American Society of
885 photogrammetry, Falls Church, 1056 pp.
886 [74] Stead, D., Eberhardt, E., Coggan, J.S. 2004. Modelling of complex rock slope failure mechanisms
887 using a hybrid finite-/discrete-element code. 1067-1072. in Landslides Evaluation and Stabilization. ISBN
888 04 1535 667 9 Proc IXth ISL, Eds Lacerda et al. Rio de Janeiro, 2004.
889 [75] Stead, D., Eberhardt, E. 2013. Understanding the mechanisms of large landslide. Vaiont 2013,
890 Italian Journal of Engineering Geology, Italian journal of engineering geology and environment. Book
891 series 6, Genevois R. and Prestininzi A. (eds.), 85 - 112
892 [76] Sturzenegger, M., Stead, D., Beveridge, A., Lee, S., van As., A. 2009. Long-range terrestrial
893 digital photogrammetry for discontinuity characterization at Palabora open-pit mine. In Diederichs M. &
894 Grasselli G. eds. "ROCKENG09: Proceedings of the 3rd CANUS Rock Mechanics Symposium", Toronto,
895 paper 3984, 10 pp.
896 [77] Sturzenegger, M., Stead, D. 2009(a). Close-range terrestrial digital photogrammetry and
897 terrestrial laser scanning for discontinuity characterization on rock cuts. Engineering Geology 106, 163-
898 182.

[78] Sturzenegger, M., Stead, D. 2009(b). Quantifying discontinuity orientation and persistence on high mountain rock slopes and large landslides using terrestrial remote sensing techniques. Natural Hazards and Earth System Sciences 9 (2), 267-287.

[79] Tonon, F., Kottenstette, J.T. 2007. Laser and photogrammetric methods for rock face characterization. Report on a Workshop Held in Golden, Colorado, June 17-18, 2006. American Rock Mechanics Association, 6 pp.

[80] Vandeginste, V., Faure, J.L., Osadetz, K., Roure, F. Swennen, R. 2012. Paleostress evolution in the Canadian Cordilleran foreland fold-and-thrust belt west of Calgary. Geologica Belgica, Vol. 15/1-2, pp. 42-52.

[81] Van Westen, C.J. 1998. GIS in landslide hazard zonation: a view, with cases from the Andes of Colombia, in: F.P. Martin, D.I. Heywood (Eds.), Mountain Environment and Geographic Information Systems, Taylor & Francis, pp. 35-165.

[82] VanWesten, C.J., Terlien, M.T.J. 1996. Deterministic landslide hazard analysis in GIS: a case study from Manizales (Colombia), Earth Surface Processes and Landforms, 21, 853-868.

[83] Wiles, t. d. 2005. Reliability of numerical modelling predictions. International Journal of Rock Mechanics and Mining Sciences, Vol. 43, 454-472

[84] Xie, M., Esaki, T., Cai M.F. 2004. A GIS-based method for locating the critical 3D slip surface in a slope, Computers and Geotechnics, 31, 267-277.

[85] Xie, M., Esaki, T., Qiu, C., Wang C.X. 2006. Geographical information system-based computational implementation and application of spatial three-dimensional slope stability analysis, Computers and Geotechnics, 33, 260-274.